

PL-TR-91-2108

AD-A240 693



2

DEVELOPMENT OF A 3-D TREE THERMAL RESPONSE
MODEL FOR ENERGY BUDGET AND SCENE SIMULATION STUDIES

John R. Hummel
James R. Jones
David R. Longtin
Nanette L. Paul

DTIC
SELECTE
SEP 19 1991
S D

SPARTA, Inc.
24 Hartwell Avenue
Lexington, MA 02173

15 March 1991

Scientific Report No. 8

Approved for Public Release; Distribution Unlimited



PHILLIPS LABORATORY
AIR FORCE SYSTEMS COMMAND
HANSCOM AIR FORCE BASE, MASSACHUSETTS 01731-5000


91 8 18 037

91-10982



"This technical report has been reviewed and is approved for publication"


ROBERT R. BELAND
CONTRACT MANAGER


DONALD E. BEDO
BRANCH CHIEF


R. EARL GOOD
DIVISION DIRECTOR

This report has been reviewed by the ESD Public Affairs Office (PA) and is releasable to the National Technical Information Service (NTIS).

Qualified requestors may obtain additional copies from the Defense Technical Information Center. All others should apply to the National Technical Information Service.

If your address has changed, or if you wish to be removed from the mailing list, or if the addressee is no longer employed by your organization, please notify PL/IMA, Hanscom AFB, MA 01731-5000. This will assist us in maintaining a current mailing list.

Do not return copies of this report unless contractual obligations or notices on a specific document requires that it be returned.

REPORT DOCUMENTATION PAGE			Form Approved OMB No. 0704 0188	
Public reporting burden for this collection of information is estimated to average 1 hour per response, including the time for reviewing instructions, searching existing data sources, gathering and maintaining the data needed, and completing and reviewing the collection of information. Send comments regarding this burden estimate or any other aspect of this collection of information, including suggestions for reducing this burden, to Washington Headquarters Services, Directorate for Information Operations and Reports, 1215 Jefferson Davis Highway, Suite 1204, Arlington, VA 22202-4302, and to the Office of Management and Budget, Paperwork Reduction Project (0704-0188), Washington, DC 20503.				
1. AGENCY USE ONLY (Leave blank)		2. REPORT DATE 15 Mar 91		3. REPORT TYPE AND DATES COVERED Scientific Report No. 8
4. TITLE AND SUBTITLE Development of a 3-D Thermal Response Model for Energy Budget and Scene Simulation Studies			5. FUNDING NUMBERS PE 62101F PR 7670 TA 15 WU AP Contract F19628-88-C-0038	
6. AUTHOR(S) John R. Hummel, James R. Jones, David R. Longtin, Nanette L. Paul				
7. PERFORMING ORGANIZATION NAME(S) AND ADDRESS(ES) SPARTA, Inc. 24 Hartwell Avenue Lexington, MA 02173			8. PERFORMING ORGANIZATION REPORT NUMBER	
9. SPONSORING / MONITORING AGENCY NAME(S) AND ADDRESS(ES) Phillips Laboratory Hanscom AFB, MA 01731-5000 Contract Manager: Robert Beland/OPA			10. SPONSORING / MONITORING AGENCY REPORT NUMBER PL-TR-91-2108	
11. SUPPLEMENTARY NOTES				
12a. DISTRIBUTION / AVAILABILITY STATEMENT Approved for public release; distribution unlimited			12b. DISTRIBUTION CODE	
13. ABSTRACT (Maximum 200 words) Energy budget modeling of vegetated surfaces is complicated by the extreme variability that can be encountered in the species that are present. A three dimensional thermal model of trees is being developed to understand the thermal properties of trees. The model is being developed for leafed (deciduous) and leafless conditions. Primitive solid geometric shapes, such as cylinders and truncated cones, are used to represent the tree trunks and branches. The material distribution within each element is then established and material properties assigned. A finite difference calculation of the energy budget is performed in which tree elements are allowed to interact with one another as well as the outside environment. This report describes the development of a three dimensional thermal response model for individual trees. The model can be used for leafed and leafless trees. The thermal balance for woody material is determined using a 3-D heat conduction model for the tree components. The thermal balance of deciduous leaves is calculated using an energy balance formulation that takes into account solar and infrared radiative interactions, free or forced convection, and evapotranspiration. Results of sensitivity calculations outlining the importance of various physical processes are given as well as comparisons against field test data.				
14. SUBJECT TERMS BTI/SWOE, Tree Thermal Response, Energy Budget			15. NUMBER OF PAGES 48	
			16. PRICE CODE	
17. SECURITY CLASSIFICATION OF REPORT UNCLASSIFIED	18. SECURITY CLASSIFICATION OF THIS PAGE UNCLASSIFIED	19. SECURITY CLASSIFICATION OF ABSTRACT UNCLASSIFIED	20. LIMITATION OF ABSTRACT SAR	

Accession For	
NTIS CRA&I	<input checked="" type="checkbox"/>
DTIC TAB	<input type="checkbox"/>
Unannounced	<input type="checkbox"/>
Justification	
By	
Distribution /	
Availability Codes	
Dist	Availability Codes
A-1	



Contents

1	INTRODUCTION	1
1.1	Background and Purpose of Research	1
1.2	Organization of Report	2
2	HEAT CONDUCTION MODEL FOR WOODY MATERIAL	2
2.1	General Approach	2
2.2	Describing the Tree Geometry	2
2.3	Developing the Computational Framework	3
2.4	Specifying the Surface Energy Budget	6
2.5	Temperature Calculations	6
2.6	Thermal Response	6
2.7	Solution Scheme	9
2.7.1	Solar Heat Flux	10
2.7.2	Radiation to Environment	11
2.7.3	Surface Convection	12
3	TREATMENT OF LEAVES	14
3.1	Leaf Attenuation	15
3.2	Calculating Leaf Temperatures	18
3.2.1	Leaf Energy Budget	18
3.2.2	Impact of Model Assumptions	19
3.2.2.1	Impact of Evapotranspiration	21
3.2.2.2	Impact of Convection	22

3.2.2.3	Impact of Leaf Diameter	22
4	VALIDATION EFFORTS	22
4.1	Overview of STAMP	22
4.2	Discussion of Results	23
4.2.1	Temperature Predictions for "Joyce Kilmer"	24
4.2.2	Trunk Temperatures for Hunter-Liggett Tree	27
5	SUMMARY AND RECOMMENDATIONS FOR FUTURE WORK	30
5.1	Summary	30
5.2	Recommendations for Future Work	30
5.2.1	Addition of Woody Material Moisture Transport	30
5.2.2	Enhancements to the Leaf Energy Budget Model	30
5.2.3	Tree-Environmental Interactions	31
	References	32
	Appendix A - Tree Shading Model	34

Figures

1	Graphical Representation of a Tree as Displayed by the Prototype User Interface System	3
2	Representing Trees as a Collection of Primitive Solid Geometric Shapes	5
3	Steps Used to Perform 3-D Thermal Calculations for Trees	5
4	Schematic Representation of the Coordinate System Used in the Heat Conductivity Calculations	7
5	Geometry and Properties Used in Determining the Thermal Resistance Between Elements i and j	8
6	Shading and Solar Attenuation due to Branches and Leaves	11
7	Schematic Representation of the Leaf Clusters	14
8	Fraction of X_c Shaded by Leaves as a Function of Incident Angle for a 4 Foot Long by 1 Foot Wide Leaf Cluster	17
9	Leaf Temperatures Calculated With and Without Evapotranspiration for Weather Conditions Representative of the FY 90 SWOE Hunter-Liggett Demonstration	21
10	Leaf Temperatures Calculated With Free and Forced Convection Assumed for Weather Conditions Representative of the FY 90 SWOE Hunter-Liggett Demonstration	22
11	Leaf Temperatures Calculated With Different Leaf Diameters Assumed for Weather Conditions Representative of the FY 90 SWOE Hunter-Liggett Demonstration	23

12	Tree Model Predictions for and Thermocouple Data From "Joyce Kilmer" for 8 and 9 September 1990	25
13	Tree Model Predictions for and Thermocouple Data From "Joyce Kilmer" for 8 and 9 September 1990	25
14	Model Temperature Cross Sections for "Joyce Kilmer" at 9 AM on 9 September 1990	26
15	Model Temperature Cross Sections for "Joyce Kilmer" at 3 PM on 9 September 1990	26
16	Predictions of the Surface Temperatures as a Function of Time for Elements Near the Cardinal Points	27
17	Model Temperature Cross Sections for 9 AM, 20 September 1989	29
18	Model Temperature Cross Sections for 3 PM, 20 September 1989	29

Tables

1	Sample of the Tree Database Collected and Assembled by the Waterways Experiment	4
2	Weather Data for the FY 90 SWOE Hunter-Liggett Demonstration	20
3	Model Conditions Assumed for Leaf Temperature Calculations	21

**Development of a 3-D
Tree Thermal Response Model for Energy Budget
and Scene Simulation Studies**

1 INTRODUCTION

1.1 Background and Purpose of Research

The Balanced Technology Initiative on Smart Weapons Operability Enhancement (BTI/SWOE) has as a goal the ability to model and study the radiant field from complex natural backgrounds. Remote sensing and modeling of vegetated surfaces is a complicated endeavor due to the extreme variability that can be encountered in the species that are present. The sizes of vegetative objects are highly variable as well as the orientations and the number of elements and components that make up the individual tree or plant.

The purpose of this study has been to develop a three dimensional thermal model of individual trees that can be used to understand the thermal properties of trees. The model, TREETHERM, is one component in the BTI/SWOE Interim Thermal Model package.¹ TREETHERM is designed to be used as a component in

¹ Hummel, J.R., Longtin, D.R., Paul, N.L., and Jones, J.R. (1991) "Development of the Smart Weapons Operability Enhancement Interim Thermal Model," Phillips Laboratory, Hanscom AFB, Lexington, Massachusetts, PL-TR-91-2073, 1991.

remote sensing simulations and as a standalone model to study the thermal response characteristics of trees to changes in environmental conditions.

1.2 Organization of Report

Section 2 describes the heat conduction model that was developed for the woody material in a tree. Section 3 describes how leaves were treated in the model. Section 4 presents results from validation efforts made with the model. Finally, Section 5 presents a summary of our efforts and recommendations for future research. A companion report provides specific details on the use of TREETHERM and the data required to run the code.²

2 HEAT CONDUCTION MODEL FOR WOODY MATERIAL

2.1 General Approach

The 3-D tree model, TREETHERM, is designed to be used in scene simulation studies and as a standalone research tool. The model can work with data for specific trees or be used to model generic trees.

In scene simulation studies, it is assumed that "standard" trees will be used for given tree types. Within a scene, the standard tree can be given different orientations. In future versions of the model it is envisioned that the standard tree could be scaled to different sizes.

2.2 Describing the Tree Geometry

The modeling philosophy taken in developing the 3-D tree model has been to adapt a formalism that would permit the user to model "generic" trees or specific trees. To achieve the latter goal, our modeling approach has been to base our 3-D geometric representation of trees on a data collection approach developed by the U.S. Army Corps of Engineers Waterways Experiment Station (WES).³

The WES database describes trees by giving the nodal information on the locations of all tree components and the starting, ending, and average diameters of the components. The nodal information is the x, y, z positions relative to a reference point where a tree element either changes direction or connects with another element. In the WES data base, x is north, y is west, and z is up. A

² Jones, J.R. (1991) "User's Guide for TREETHERM: A 3-D Thermal Model for Single Trees," Phillips Laboratory, Hanscom AFB, Massachusetts, PL-TR-91-2109, 31 March 1991.

³ West, H.W., and Allen, H.H. (1971) "A Technique for Quantifying Forest Stands for Management Evaluations", US Army Engineer Waterways Experiment Station, Vicksburg, MS, Technical Report M-71-9, December 1971.

sample of the data is shown in Table 1. A prototype user interface system has also been developed for our 3-D tree thermal model. One option in the system is to access the database and display a graphical representation of the tree being modeled. Figure 1 shows a display from a prototype user interface system that was developed for TREETHERM.

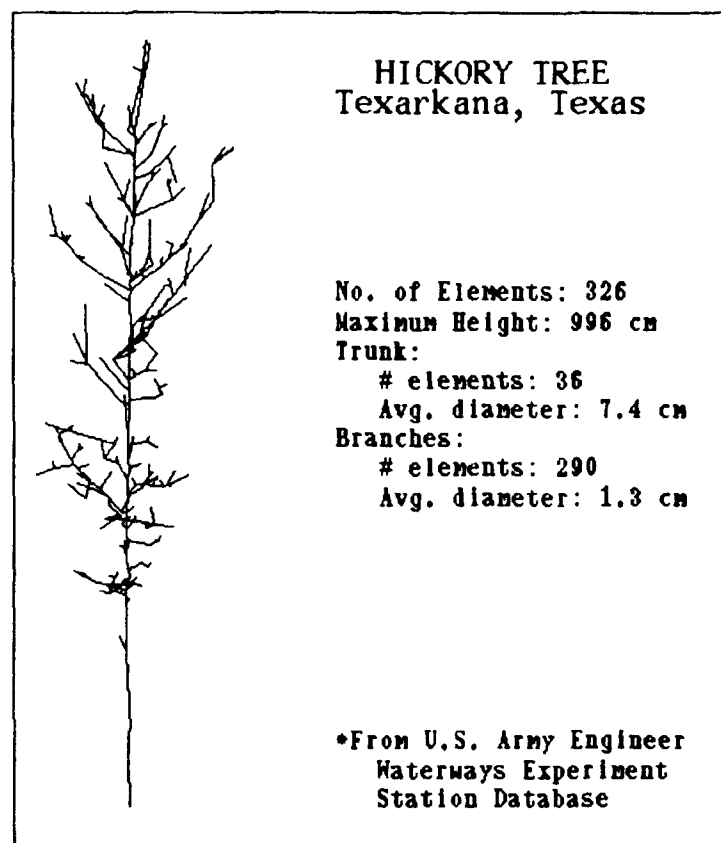


Figure 1. Graphical Representation of a Tree as Displayed by the Prototype TREETHERM User Interface System

2.3 Developing the Computational Framework

Once the data for a tree have been assembled, the tree components are modeled via a solid modeling technique in which primitive geometric shapes are used for each component, as shown in Figure 2. In our model, truncated cylinders are the shapes being used to represent the tree components. The components are then divided into standardized parts, such as trunk, limbs, branches, twigs, etc. Once the parts are identified, the material distribution within each part is established, as

Table 1. Sample of the Tree Database Collected and Assembled by the Waterways Experiment Station. (The number trunk and branch elements was determined from the data and is not a part of the WES data.)

Node #	SOURCE				Node #	TERMINUS				Avg. Stem Diam (cm)
	X Coord (cm)	Y Coord (cm)	Z Coord (cm)	Diam (cm)		X Coord (cm)	Y Coord (cm)	Z Coord (cm)	Diam (cm)	
1	1379.0	284.0	13.0	19.7	2	1376.0	280.0	81.0	16.5	18.1
3	1376.0	280.0	81.0	16.5	4	1380.0	287.0	156.0	12.0	14.2
5	1380.0	287.0	156.0	12.0	6	1375.0	287.0	231.0	11.3	11.6
7	1375.0	287.0	231.0	1.4	8	1363.0	311.0	246.0	0.7	1.1
9	1375.0	287.0	231.0	11.3	10	1375.0	293.0	299.0	9.9	10.6
11	1374.0	293.0	299.0	2.5	12	1378.0	306.0	297.0	1.7	2.1
13	1378.0	306.0	297.0	0.6	14	1377.0	305.0	300.0	0.4	0.5
15	1378.0	306.0	297.0	0.6	16	1376.0	305.0	295.0	0.4	0.5
17	1378.0	306.0	297.0	0.9	18	1375.0	302.0	297.0	0.7	0.8
19	1375.0	293.0	299.0	1.7	20	1374.0	293.0	317.0	9.2	5.4
21	1374.0	293.0	317.0	2.8	22	1388.0	307.0	319.0	2.5	2.7
23	1388.0	307.0	319.0	2.1	24	1336.0	287.0	321.0	1.7	1.9
25	1336.0	287.0	321.0	1.7	26	1319.0	283.0	328.0	1.5	1.6
27	1319.0	283.0	328.0	0.8	28	1315.0	289.0	330.0	0.7	0.7
29	1319.0	283.0	328.0	1.5	30	1316.0	283.0	329.0	1.5	1.5
31	1316.0	283.0	329.0	1.2	32	1300.0	290.0	338.0	0.8	1.0
33	1316.0	283.0	329.0	1.5	34	1289.0	294.0	339.0	0.5	1.0
35	1370.0	278.0	316.0	2.3	36	1349.0	302.0	317.0	2.1	2.2
37	1349.0	302.0	317.0	2.1	38	1356.0	337.0	323.0	1.8	2.0
39	1356.0	337.0	323.0	1.3	40	1345.0	343.0	325.0	0.6	0.9
41	1356.0	337.0	323.0	1.4	42	1360.0	361.0	325.0	0.9	1.1
43	1374.0	293.0	317.0	10.3	44	1378.0	297.0	332.0	9.7	10.0
45	1378.0	297.0	332.0	2.6	46	1365.0	260.0	327.0	2.4	2.5
47	1365.0	260.0	327.0	2.0	48	1367.0	255.0	329.0	1.5	1.8
49	1367.0	255.0	329.0	0.8	50	1371.0	260.0	333.0	0.6	0.7
⋮					⋮					

shown as Step 1 in Figure 3. In this version of the tree model, the internal material distribution is assumed to be isotropic. The radii of the cylinders denoting the different woody materials are user inputs² and can vary from tree to tree and between tree components.

Different material properties can be assigned to the different tree components. The material properties can vary from segment to segment. This feature would allow one to model the presence of dead material on a living tree. The material properties can also be treated as temperature dependent. Within each modeled cylindrical segment the material distribution is assumed to be homogeneous.

This version does not treat the flow of moisture within the tree. However, this can be examined, at least to a first approximation, by the model's ability to vary material properties by position.

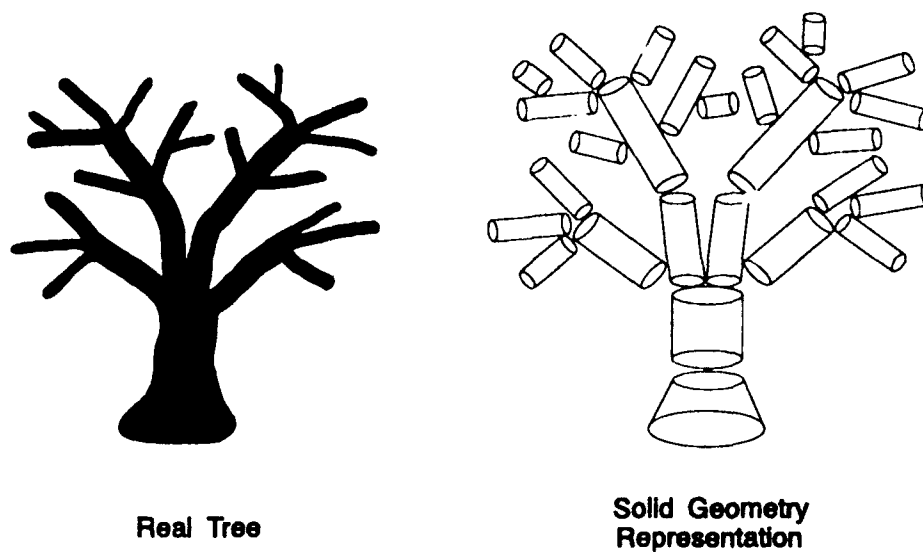


Figure 2. Representing Trees as a Collection of Primitive Solid Geometric Shapes

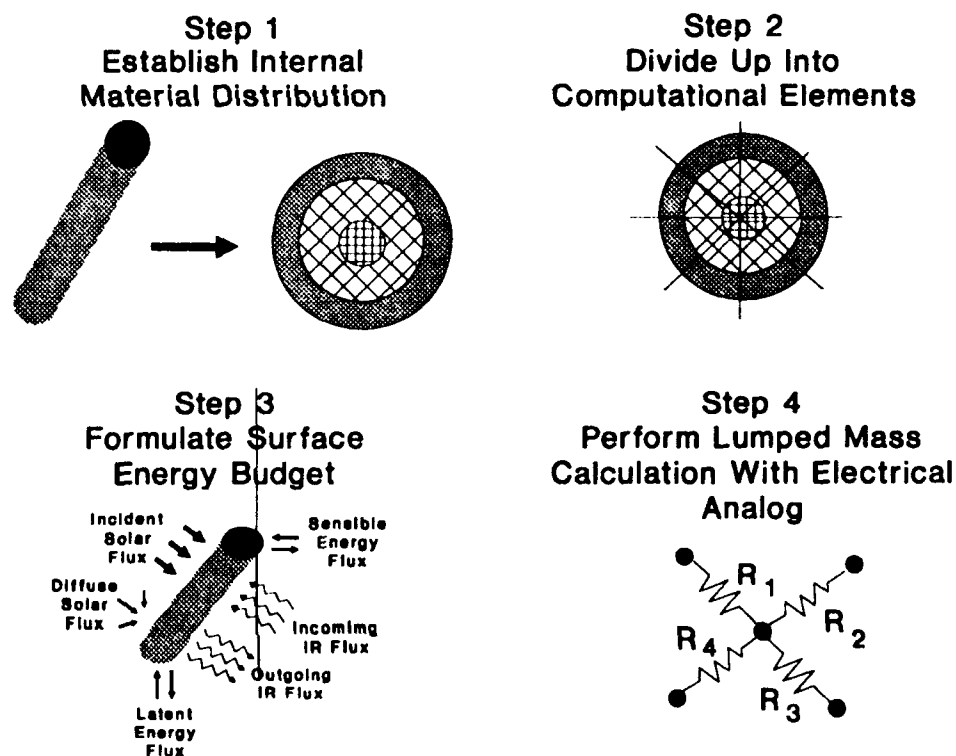


Figure 3. Steps Used to Perform 3-D Thermal Calculations for Trees

Each tree component is divided into cylindrical subcomponents and each sub-component is then divided into computational elements, as shown as Step 2 in Figure 3.

2.4 Specifying the Surface Energy Budget

The surface energy budget, as shown as Step 3 in Figure 3, is formulated in terms of the incoming solar and infrared, reradiation to the atmosphere, convective and latent terms, and conduction into the material. Direct and diffuse solar fluxes are attenuated through the leafy canopy and reflected off of the bark. Self-shading from the various tree components are also considered via the use of a ray-tracing routine. The tree shading model uses ray casting technology initially implemented in SPARTA's Optical Sensor Simulation (SENSORSIM)^{4,5,6} for rendering images or signatures of various objects as observed by optical sensor systems. The convective term is treated in terms of the energy transfer resulting from air flow around cylindrical surfaces.

2.5 Temperature Calculations

The temperatures are calculated at the radial mid-point of each element and applied throughout the element. The heat conduction calculations are performed using the "lumped mass" approach and an electrical analog, as noted as Step 4 in Figure 3. This approach is similar to that done in a study by Derby and Gates.⁷ Each element typically interacts with up to six adjacent nodes.

2.6 Thermal Response

The thermal response of the model will be in three spatial dimensions (x, y, z) predicted from the general heat balance equation for a nonhomogeneous, anisotropic material is given by

$$\rho c \frac{\partial T}{\partial t} = \frac{\partial}{\partial x} \left(k_x \frac{\partial T}{\partial x} \right) + \frac{\partial}{\partial y} \left(k_y \frac{\partial T}{\partial y} \right) + \frac{\partial}{\partial z} \left(k_z \frac{\partial T}{\partial z} \right) + Q(x, y, x, t) \quad (1)$$

where ρ is the density of the woody material in kg m^{-3} ; c is the specific heat of the material in $\text{J kg}^{-1} \text{K}^{-1}$; T is the temperature in K; t is the time in seconds; $k_x, k_y,$

⁴ Guivens, Jr., N.R., and Henshaw, P.D. (1986) "Laser Radar Sensor Model," SPARTA, Inc., Lexington, MA, SPARTA LTR-86-08, 27 June 1986.

⁵ Guivens, Jr., N.R., and Henshaw, P.D. (1986) "Laser Radar Sensor Simulation," SPARTA, Inc., Lexington, MA, SPARTA LTR-87-011, 26 November 1986.

⁶ Henshaw, P.D., and Guivens, Jr., N.R. (1987) "Active/Passive Multiwavelength Imaging Sensor Simulation," *Laser Radar II*, R. J. Becherer and R. C. Harney, Ed., Proc. SPIE 783:84-90.

⁷ Derby, R.W., and Gates, D.M., (1966) The Temperature of Tree Trunks - Calculated and Observed, *Amer. J. Bot.*, 53:580-587.

and k_z are the conductivities in the x, y, z directions, respectively, in $\text{W m}^{-1} \text{K}^{-1}$; and $Q(x, y, z, t)$ is the net summation of the surface energy fluxes.

In this initial version of TREETHERM, the tree elements will be modeled by the lumped mass approach for cylindrical segments. Therefore, the x, y, z directions above will correspond to the radial, circumferential, and longitudinal (axial) directions, respectively, as shown in Figure 4.

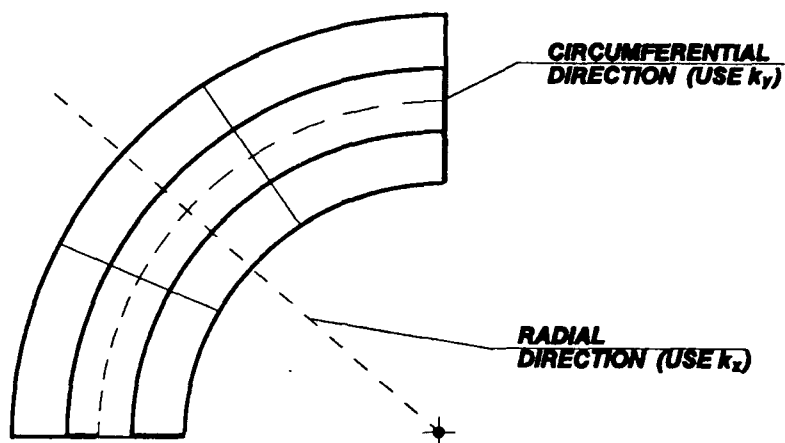


Figure 4. Schematic Representation of the Coordinate System Used in the Heat Conduction Calculations

The Crank-Nicholson finite difference method is used to approximate the partial derivatives in the energy balance equation. This approach gives more accurate results than the fully implicit or explicit methods. In general, the solution scheme is unconditionally stable, but can be subject to oscillations.⁸

The coefficients obtained from the Crank-Nicholson procedure are used to solve for the element temperatures using a modified Seidel iterative scheme. The numerical implementation of the heat balance is taken from Duncan *et al.*⁹

The finite difference form of Eqn. 1 is

$$\frac{\rho_i c_i V_i}{\Delta t} (T'_i - T_i) = \sum_{\substack{j=1 \\ j \neq i}}^n \left(C_{ij} \left[\frac{(T'_j + T_j)}{2} - \frac{(T'_i + T_i)}{2} \right] \right) + Q_i \quad (2)$$

where i is the number of the element being solved for, j is the number of the

⁸ Carnahan, B. Luther, H.A., and Wilkes (1969) Applied Numerical Methods, Wiley & Sons, New York, p.451.

⁹ Duncan, T.C., Farr, J.L., Wassel, T., and Curtis, R.J., Satellite Laser Vulnerability Model, Thermal Model User's Guide, Air Force Weapons Laboratory, (Software Documentation).

element in thermal contact with element i , n is the total number of elements in thermal contact with i , Δt is the time step in seconds, V is the volume of element j in m^3 , T_i and T_j are the previous temperatures in K for elements i and j , T'_i and T'_j are the temperatures being solved for, C_{ij} is the heat conduction parameter in W K^{-1} , and Q_i is the total surface flux at element i . Thermal contact means that energy may be transferred between elements by conduction.

The heat conduction parameter is determined from an electrical analog, the lumped mass approach, and given in terms of a thermal resistance, R_{ij} ,

$$C_{ij} = \frac{1}{R_{ij}} \quad (3)$$

where the thermal resistance is given by

$$R_{ij} = \frac{L_{ij}}{k_i A_{ij}} \quad (4)$$

In the above, the thermal resistance, in K W^{-1} , is evaluated (see Figure 5) from the center or radial midpoint of element i to the surface of i in contact with the adjacent element j . This distance is L_{ij} and is given in meters. k_i is the thermal conductivity in $\text{W m}^{-1} \text{K}^{-1}$ of element i in the element j direction, and A_{ij} is the average cross-sectional area in m^2 between the calculation location of i to the surface of i in contact with j . The lumped mass electrical analog has the advantage of handling arbitrary shapes and element connections.

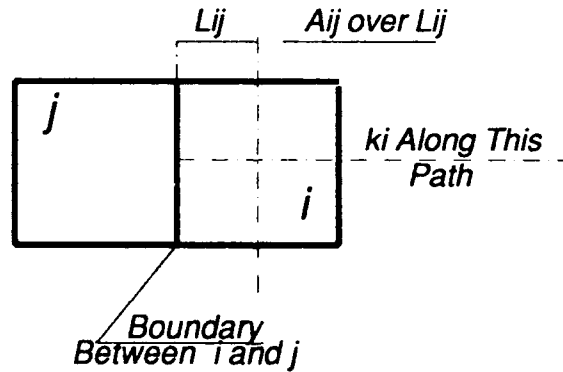


Figure 5. Geometry and Properties Used in Determining the Thermal Resistance Between Elements i and j

It should be noted that the current version of TREETHERM can handle temperature dependent properties for the specific heat, conductivity, emissivity, and absorptivity. This version does not attempt a mass balance due to moisture transport within the tree. Also, water content is not directly considered. Its effect can

be approximated by changing the material properties used, however. Including the effects of moisture transport is planned for future versions of the model.

The implementation of the energy balance (Eqn. 2) has the advantage of allowing each element being modeled to have different boundary fluxes applied to it. For the current version of TREETHERM, these boundary fluxes are permitted only at surface elements. The surface conditions currently modeled are the solar energy, surface reradiation to environment, and surface convection due to wind.

2.7 Solution Scheme

TREETHERM uses an adaptive time step in its solution scheme. The time step is controlled by convergence criteria in the solution scheme and a maximum allowable temperature change for each element (1.5 K) over a calculation time interval.

If the solution for a time step does not converge within the iteration limit (200 steps), the model retreats to the start of the time interval, resets time dependent parameters, reduces the time step, and repeats the calculation. If the solution converges, the magnitude of each element's temperature change is compared to the maximum allowed temperature change. If any element's temperature change over the time step exceeds the allowable, the calculation will be repeated with the time step reduced. This time step reduction for the repeat calculation will take into account the amount by which the temperature change criteria was exceeded. If the calculation for a time step is repeated over a certain number of intervals (100 steps), a warning is issued about subsequent results and the calculation allowed to advance in time.

If the solution converges and the element temperature change criteria are met, the model updates the applicable parameters and advances in time by the current time step. The scheme will try to increase the time step for the next calculation based on the ratio of the maximum element temperature change to the allowable element temperature change for the previous time step. To avoid excess repeat calculations, the maximum increase in a time step over a previous time step is limited to 10 per cent. A time step is also subject to a maximum of 300 seconds and a minimum of 1 second. The minimum allowed time step can be circumvented when the model is trying to hit a meteorological data time interval.

The temperature increase criteria and the maximum and minimum allowed time step values are based on a variety of factors. These factors include the expected range of tree material properties and environmental boundary conditions, convergence in the solution scheme, and expected meteorological data interval times, as well as exercising the code for various combinations of temperature increase and time step criteria.

The solution iteration and repeat calculation limits are conservative for the expected combination of tree material properties and environmental boundary conditions. These limits are applicable to the general purpose three dimensional thermal code from which TREETHERM is derived. This approach is also used in the SWOETHERM portion of the BTI/SWOE Interim Thermal Model (ITM).¹

2.7.1 Solar Heat Flux

The solar heat flux is a time and spatial varying energy source. It can be obtained from data or estimated from various radiative transfer parameterizations. The approach used in TREETHERM is the same as that used in the Interim Thermal Model.¹

The solar flux incident on the tree elements are separated into direct and diffuse components. The diffuse part is treated as radially symmetric to a given tree segment. The total solar heat flux in W m^{-2} absorbed by a surface element, Q_{HF_i} , is given as

$$Q_{HF_i} = \alpha_i [S_{dr}(x, y, z, t) A_i \cos \theta_i + S_{df}(x, y, z, t) A_{idf}] \quad (5)$$

where $S_{dr}(x, y, z, t)$ and $S_{df}(x, y, z, t)$ are the direct and diffuse solar energy, respectively, on element i ; α_i is the surface absorptivity of element i ; A_i is the area of element i receiving the direct solar energy; A_{idf} is the area of element i receiving the diffuse solar energy; and θ_i is the angle of incidence between the surface normal for element i and the solar vector.

Shading due to leaves and branches as well as attenuation by the leaves can modify the solar energy incidence on a surface element. These effects are handled via an adaptive ray casting scheme that is discussed in Appendix A. The ray casting scheme determines the illuminated area of branches projected onto the solar vector line of sight with an attenuation modification if leaves are present in the model. Section 3 of this report details the modeling of the leaf energy transmission. Figure 6 presents some of the possible outcomes of a set of rays cast through a tree model.

The shading/attenuation effects will change as a function of time of day. However, within TREETHERM they are implemented at the midpoint of the time interval for the meteorological data containing the solar fluxes rather than at every computational timestep. This is done primarily for computational reasons. The raycasting approach is very computationally intensive and results in a significant increase in computational times. The approach used here is believed to be acceptable considering the uncertainties in tree and leaf material properties, environmental conditions, leaf and orientation variations due to wind speed changes, etc.

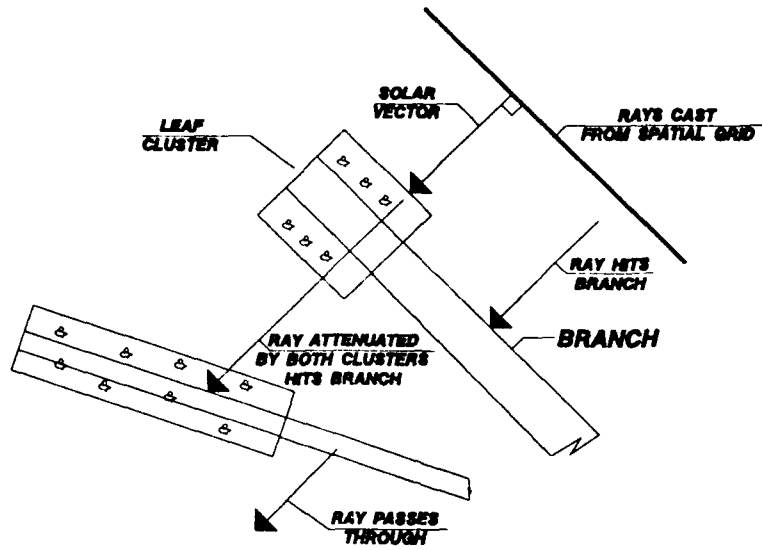


Figure 6. Shading and Solar Attenuation due to Branches and Leaves

2.7.2 Radiation to Environment

Currently, the tree model has two implementations of surface re-radiation. First, the surface elements can radiate to a background temperature. This method is used if the downward infrared data are not available from the meteorological data and the built-in infrared parameterization is disabled. In this case, the expression for the reradiation is

$$Q_{REi} = \epsilon_i A_i S F_i \sigma (T_{\infty}^4 - T_i^4) \quad (6)$$

where Q_{REi} is the infrared radiation to the background environment from element i , ϵ_i is the emissivity of the surface element i , A_i is the area in m^2 of the radiating surface, $S F_i$ is the shape factor (which is 1 in this version), σ is the Stefan-Boltzmann constant, and T_{∞} is the background temperature in K obtained from the meteorological data. The second method of determining the net re-radiation at a surface is

$$Q_{REi} = \alpha_{iIR} A_i IR - \epsilon_i A_i S F_i \sigma T_i^4 \quad (7)$$

where IR is the downwelling infrared flux from the atmosphere in W m^{-2} .

The infrared flux from the ground is not modeled here. An approximation to this is done by letting the downward atmospheric infrared flux be spherically symmetric. Then, adjustments can be made to the material infrared surface absorptivity. That is, those computational elements that face the ground can have

an infrared surface absorptivity different than those facing the sky. In future versions of TREETHERM, the upwelling infrared flux from a thermal model of the underlying ground will be added.

2.7.3 Surface Convection

The heat transfer between the surrounding air and a given surface element of a tree segment is given as

$$Q_{SC_i} = h_i A_i (T_\infty - T_i) \quad (8)$$

where Q_{SC_i} is the surface convection at element i , h_i is the convective coefficient at element i in $\text{W m}^{-2} \text{K}^{-1}$, and A_i is the surface area of element i in m^2 .

The coefficient for forced convection, which occurs when the wind speed is not zero, is determined from Churchill's correlation equations for cylinders as^{10,11}

$$h_i = \frac{\overline{Nu_D} k_f}{D} \quad (9)$$

where $\overline{Nu_D}$ is the mean Nusselt number, k_f is the fluid (air) conductivity in $\text{W m}^{-1} \text{K}^{-1}$, and D is the cylinder diameter in m. The mean Nusselt number is determined as a function of the Reynolds number, Re_D ; Prandtl number, Pr ; or Peclet number, Pe . For example,

$$\overline{Nu_D} = 0.3 + \frac{0.62 Re_D^{\frac{1}{2}} Pr^{\frac{1}{3}}}{\left[1 + (0.4/Pr)^{\frac{2}{3}}\right]^{\frac{1}{4}}} \quad Re_D \leq 4000 \quad (10)$$

$$\overline{Nu_D} = 0.3 + \frac{0.62 Re_D^{\frac{1}{2}} Pr^{\frac{1}{3}}}{\left[1 + (0.4/Pr)^{\frac{2}{3}}\right]^{\frac{1}{4}}} \left[1 + \left(\frac{Re_D}{282,000}\right)^{\frac{1}{2}}\right] \quad 20,000 < Re_D < 400,000 \quad (11)$$

$$\overline{Nu_D} = 0.3 + \frac{0.62 Re_D^{\frac{1}{2}} Pr^{\frac{1}{3}}}{\left[1 + (0.4/Pr)^{\frac{2}{3}}\right]^{\frac{1}{4}}} \left[1 + \left(\frac{Re_D}{282,000}\right)^{\frac{5}{8}}\right]^{\frac{4}{5}} \quad \text{General Case} \quad (12)$$

¹⁰ Churchill, S.A., and Bernstein, M. (1977), A Correlating Equation for Forced Convection from Gases and Liquid to a Circular Cylinder in Crossflow, *J. Heat Transfer*, **99**:300-306.

¹¹ Lienhard, J. M., (1981), *A Heat Transfer Textbook*, Prentice-Hall, Englewood Cliffs, NJ, 1981, pp 326-337.

$$\overline{Nu_D} = \frac{1}{0.8237 - \ln\left(Pe^{\frac{1}{2}}\right)} \quad Pe \leq 0.2 \quad (13)$$

The expressions for the Nusselt number given above are based on empirical observations. (The reader is referred to any standard text on heat transfer for a discussion of the above parameters.) The Reynolds number is given as

$$Re_D = uD/\nu \quad (14)$$

where u is the free stream (wind) velocity in m/s, D is the diameter of the cylinder in m, and ν is the fluid (air) kinematic viscosity in $m^2 s^{-1}$. The Prandtl number is given as

$$Pr = \nu/\alpha \quad (15)$$

where α is the fluid (air) diffusivity in $m^2 s^{-1}$. Finally, the Peclet number is given as

$$Pe = Pr \cdot Re_D. \quad (16)$$

Eqn. 12 is given as the correlating equation over the entire range of Re_D , and Eqns. 10 and 11 are used for the typical applications used in TREETHERM. Eqn. 13 is recommended when the Peclet number is less than 0.2.

It is recognized that the forced convective term h_i will vary circumferentially. Giedt¹² has provided a range of experimental data to estimate h_i as a function of radial location from the stagnation point. These data were used in a study of temperature variation in tree trunks⁷ and are similar to those calculated by the model. This method will be included as an alternative to the current convective estimation in a subsequent version of the tree model.

A free convective term has not yet been incorporated into the convective heat transfer term. However, a modification factor can be applied to the Nusselt number to account for a small amount of assisting or opposing free convection.^{10,13}

¹² Giedt, W. H., (1949), Investigation of Variation of Point Unit Heat-Transfer Coefficient Around a Cylinder Normal to an Air Stream, *Trans. ASME*, **71**:375-381.

¹³ Churchill, S. W., (1977), A Comprehensive Correlating Equation for Laminar, Assisting, Forced and Free Convection, *AIChE Journal*, **23**:10-16.

3 TREATMENT OF LEAVES

The tree geometry database used to describe a given tree can contain the positions of leaf clusters on branches. Currently, we are only considering deciduous trees. Future versions of TREETHERM will be expanded to include coniferous trees.

We are assuming that the leaves occur in cylindrical clusters around the branch segments, as shown in Figure 7. We are also assuming that the leaves are uniform in size within each cluster, the clusters have a medium density of leaves, and that the leaves are well ventilated. In this version of TREETHERM, the leaves are treated as flat plates and are assumed to be randomly oriented relative to tree elements for all wind speeds. This will be examined in later versions of the model, however.

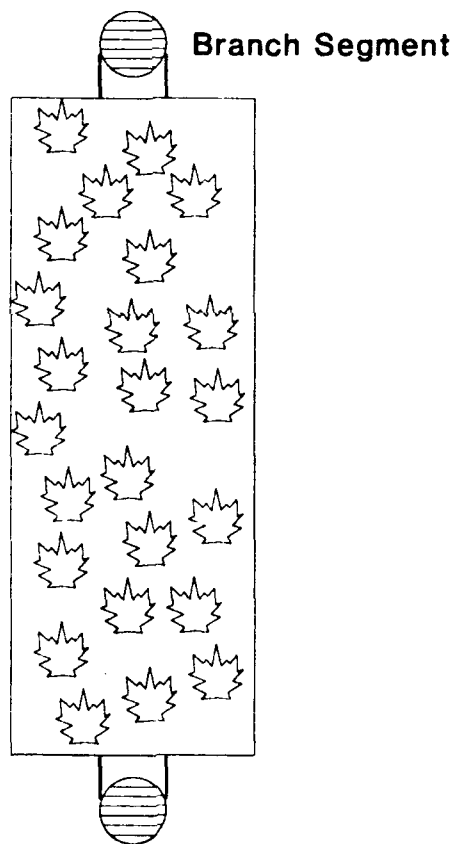


Figure 7. Schematic Representation of the Leaf Clusters

3.1 Leaf Attenuation

The attenuation of radiation by the leaf clusters is being treated with an aerosol attenuation analog. Specifically, the leaf attenuation model calculates macroscopic attenuation properties by summing the attenuation effects from individual leaves making up the cluster. The macroscopic attenuation properties account for gaps in leaf clusters and leaf overlapping as described below.

The general approach is to model a leaf cluster as a cylindrical envelope containing leaves and air where the parent branch segment is the symmetry axis. The observed geometry of individual leaves is then used to construct macroscopic values of transmittance, T_c , absorptance, A_c , and reflectance, R_c , for the leaf cluster. Physically, these macroscopic values represent the fraction of energy transmitted through, absorbed in, and reflected by the leaf cluster as a whole. Additionally, the macroscopic transmission to the parent branch, T_{br} , is also calculated. Any ray encountering a leaf cluster will interact according to these macroscopic amounts. (More precise modeling would require detailed information about the internal structure of leaf clusters which is beyond the scope of this effort.) The macroscopic parameters of the leaf clusters have the properties

$T_c(\theta)I_o$ = Radiation Transmitted Through A Cluster

$A_c(\theta)I_o$ = Radiation Absorbed In A Cluster

$R_c(\theta)I_o$ = Radiation Reflected By A Cluster

$T_{br}(\theta)I_o$ = Radiation Transmitted To A Parent Branch

where I_o is the incident radiation and θ is the angle between the parent branch segment and the incident ray. Due to symmetry arguments, the macroscopic parameters have the property that $T_c(\theta) = T_c(180 - \theta)$, for example. The angular dependence arises because the potential shading area of a cluster depends on the direction of the incident radiation. When the incident ray is along the symmetry axis, for example, leaves cast their shadow into the area defined by the circular face of the cylinder. Similarly, when the incident ray is normal to the symmetry axis, leaf shadows are in a rectangular area defined by the diameter and length of the cylinder. Formally, the potential shading area of a cylindrical cluster, X_c in cm^2 , is

$$X_c(\theta) = \pi r^2 \cos \theta + 2rl \sin \theta \quad (17)$$

where r and l are the radius and length of the cluster, respectively. For T_{br} however, it is necessary to describe the radiation passing through the plane containing the parent branch. Here, the potential shading area is the projection of the rectangle defined by

$$X_{br}(\theta) = 2rl \sin \theta. \quad (18)$$

As a result of the assumption of symmetry, there is no azimuthal dependence on either X_c or X_{br} .

To develop macroscopic leaf parameters, individual aspen leaves, for example, are assumed to be uniform circular plates each having a surface area of 30 cm^2 . The leaf number density is taken as 30 leaves per foot of leaf cluster. (In TREETHERM, the surface area of individual leaves and the leaf number density are user supplied inputs.) Due to the strong influence of wind, it is assumed that individual leaves are randomly oriented inside the cylindrical cluster. Specifically, the shadowed area casted by an individual leaf, $X_l(\phi)$ in cm^2 , is

$$X_l(\phi) = 30 \cos \phi \quad (19)$$

where ϕ , which randomly varies between 0 and 90 degrees, is the angle between the incident radiation and the normal to the leaf plate. Partial leaf overlapping is also addressed by means of a statistical approach. To do this, individual leaves are randomly placed on $X_c(\theta)$ such that the total area shaded by leaves is

$$S_c(\theta) = \sum_{i=1}^n \begin{cases} X_l^i(\phi) & \varepsilon_i > S_c^{i-1}(\theta) / X_c(\theta) \\ o_i X_l^i(\phi) & \varepsilon_i < S_c^{i-1}(\theta) / X_c(\theta) \end{cases} \quad (20)$$

where n is the number of leaves, ε_i and o_i are random numbers between 0 and 1, and $S_c^{i-1}(\theta) / X_c(\theta)$ is the cumulative fractional shading up to the $i - 1$ leaf. Implicit in the above expression is that leaves can be placed anywhere within the cylindrical envelop. Physically, this is a reasonable assumption given that 1.) leaf stems vary in length and 2.) leaves and their stems are often bent such they are close to the parent branch during windy conditions.

It also follows that the area covered by overlapping leaves is given by

$$O_c(\theta) = \sum_{i=1}^n (1 - o_i) X_l^i(\phi) \quad \varepsilon_i < S_c^{i-1}(\theta) / X_c(\theta). \quad (21)$$

Future leaf modeling efforts will modify Eqn 19 and 21 to account for diffraction effects around leaf edges which tend to blur the shadow casted by an individual leaf.

The above expressions for $S_c(\theta)$ and $O_c(\theta)$ have been evaluated for a leaf cluster 4 feet long by 1 foot wide. Figure 8 shows these results as a function of incident angle (θ) where $S_c(\theta)$ and $O_c(\theta)$ have been normalized by $X_c(\theta)$. The model suggests that about 60 percent of X_c is shaded when incident rays encounter the cluster lengthwise ($40 \leq \theta \leq 90 \text{ deg}$) which reasonably agrees with visual observations made of an aspen used in our validation studies (see Section 4.) The amount of shading and overlapping increases when incident angles decrease

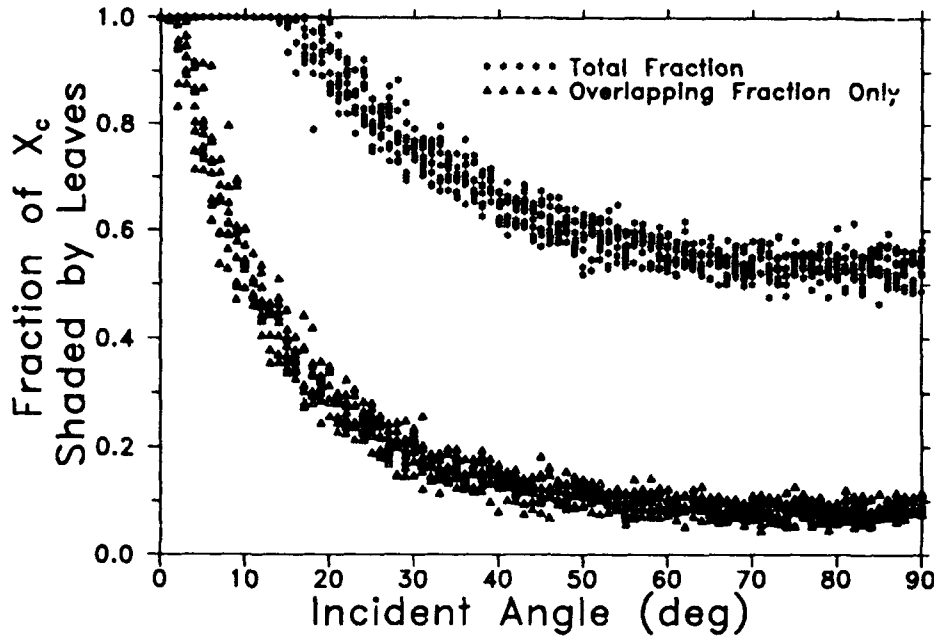


Figure 8. Fraction of X_c Shaded by Leaves as a Function of Incident Angle for a 4 Foot Long by 1 Foot Wide Leaf Cluster. The fraction shading by overlapping leaves is also shown in the Figure

from 40° to 20° . Below about 20° , where the rays are directed along the parent branch axis, X_c is completely shadowed by leaves.

The above expressions for leaf shading can be used to obtain the macroscopic transmission coefficient for a leaf cluster

$$T_c(\theta) = \frac{(X_c(\theta) - S_c(\theta) + t_l(S_c(\theta) - O_c(\theta)) + t_l^2 O_c(\theta))}{X_c(\theta)} \quad (22)$$

where t_l is the transmission for an individual leaf. (Angular variations in t_l are not considered in this effort.) Effectively, the individual terms in the above expression represent weighted averages of the areas covered by no leaves, single leaves and overlapping leaves. The overlapping leaf term assumes incident rays encounter two leaves before exiting which may not be valid for dense leaf clusters. Also the shading effects of the parent branch are assumed negligible. Similar expressions can be developed for the macroscopic absorption and reflection coefficients

$$A_c(\theta) = \frac{(a_l S_c(\theta) + a_l t_l O_c(\theta))}{X_c(\theta)} \quad (23)$$

$$R_c(\theta) = \frac{(r_l S_c(\theta) + r_l t_l O_c(\theta))}{X_c(\theta)} \quad (24)$$

where a_l and r_l are the absorption and reflection for an individual leaf. The

macroscopic parameters have the property $T_c(\theta) + A_c(\theta) + R_c(\theta) = 1$.

The radiation transmitted to a parent branch, T_{br} , is given by

$$T_{br}(\theta) = \frac{(X_{br}(\theta) - S_{br}(\theta) + t_l(S_{br}(\theta) - O_{br}(\theta)) + t_l^2 O_{br}(\theta))}{X_{br}(\theta)} \quad (25)$$

where X_{br} is given by Eqn 18, S_{br} is the leaf shading in the plane containing the parent branch, and O_{br} is the area covered by overlapping leaves in the plane containing the parent branch. The leaf shading, S_{br} , is given by

$$S_{br}(\theta) = \sum_{i=1}^{n/2} \begin{cases} X_l^i(\phi) & \varepsilon_i > S_{br}^{i-1}(\theta) / X_{br}(\theta) \\ o_i X_l^i(\phi) & \varepsilon_i < S_{br}^{i-1}(\theta) / X_{br}(\theta) \end{cases} \quad (26)$$

and O_{br} is given by a form similar to Eqn 21.

3.2 Calculating Leaf Temperatures

3.2.1 Leaf Energy Budget

The leaf energy budget model is based on a formulation of Gates¹⁴ for a single leaf. The energy budget is given as

$$\frac{\alpha_{dr}(S+s) + \alpha_{df}r_s(S+s)}{2} + \frac{\alpha_t(R_a + R_g)}{2} - \epsilon_t \sigma T_\ell^4 \pm C \pm LE = 0 \quad (27)$$

where α_{dr} is the leaf absorptance to direct solar radiation, α_{df} is the leaf absorptance to diffuse solar radiation, S is the direct solar flux, s is the diffuse solar flux, r_s is the surface albedo, α_t is the leaf infrared absorptance, R_a is the downwelling infrared radiation from the atmosphere, R_g is the upwelling infrared radiation from the underlying ground, ϵ_t is the leaf infrared emittance, σ the Stefan-Boltzmann constant, T_ℓ is the leaf temperature, C is the convective exchange term, L is the latent heat of vaporization, and E is the evapotranspiration term.

The convective exchange term is given as¹⁴

$$C = h_c(T_\ell - T_a) \quad (28)$$

where h_c is the convection coefficient and T_a is the air temperature. The convection coefficient is dependent upon the shape, orientation, and size of the leaf; the state of the air flow (laminar or turbulent); whether the convection is free or forced; and upon any interactions between leaves. For the purposes of this study, the leaves will be treated as circular flat plates that have minimal interactions with one another and are oriented into the wind. In the case of free convection in still air, h_c can be given as¹⁴

¹⁴ Gates, D.M. (1964) "Characteristics of Soil and Vegetated Surfaces to Reflected and Emitted Radiation," Proceedings IGARD Symposium on Remote Sensing of Environment, 573-600.

$$h_c = 4.19 \left[\frac{T_\ell - T_a}{d_\ell} \right]^{\frac{1}{4}} \quad (29)$$

where d_ℓ is the leaf diameter. For forced convection, h_c is given as¹⁴

$$h_c = 3.98 \left(\frac{V}{d_\ell} \right)^{\frac{1}{2}} \quad (30)$$

where V is the wind speed.

The evaporation of water from a leaf occurs as a process of water vapor diffusion from the saturated inner cells through the leaf stomata and across the leaf boundary layer to the free air. The rate of water vapor diffusion, E , is proportional to the gradient of water vapor density between the leaf and the free air. This can be expressed as

$$E = \frac{\rho_S(T_\ell) - rh\rho_S(T_a)}{R} \quad (31)$$

where ρ_S is the saturation water vapor density at the leaf temperature, rh is the relative humidity of the ambient air, $\rho_S(T_a)$ is the saturation water vapor density of the air, and R is the diffusion resistance of the leaf. The diffusion resistance depends upon the leaf morphology of the given species. Gates¹⁴ gives a characteristic value of 6.0 sec cm^{-1} for many deciduous species in full sunlight with the stomates wide open. In contrast, the diffusion resistance for conifers is given by Gates as 30.0 sec cm^{-1} or greater. The diffusion resistance should be treated as temporally dependent but, for the purposes of this first generation model, will be treated as a constant.

3.2.2 Impact of Model Assumptions

Representative leaf temperatures were calculated using weather conditions at Hunter-Liggett, California, on 20 September 1989. This was the day chosen for the FY 90 BTI/SWOE demonstration. The day was a clear day. Table 2 lists the weather data for the day and Table 3 lists the default parameters used in the leaf temperature calculations. The surface albedo is representative of bare surfaces or surfaces with light vegetation.¹⁵ The leaf solar absorptances are representative of a variety of plants.¹⁶

¹⁵ Hummel, J.R., and Reck, R.A. (1979) A Global Surface Albedo Model, *J. Appl. Meteor.*, 18:239-253.

¹⁶ Gates, D.M., Kegan, H.J., Schleter, J.C., and Weidner, V.R. (1965) Spectral Properties of Plants, *Appl. Optics*, 4:11-20.

Table 2. Weather Data for the FY 90 SWOE Hunter-Liggett Demonstration. The data are for Julian Day 263, 20 September 1989

TIME (LST)	TEMP (C)	RH (%)	VISIBILITY (km)	CLOUD OBS	CLOUD COVER (%)	WIND SPEED (m/sec)	WIND DIRECTION (deg)	SURFACE PRESS (mb)
0100	10.6	89	25	Clear	0	0.31	128	968.8
0200	10.5	90	25	Clear	0	0.67	76	969.2
0300	9.4	90	25	Clear	0	0.05	Calm	969.2
0400	9.5	91	25	Clear	0	0.21	91	969.4
0500	8.7	91	25	Clear	0	0.62	56	969.6
0600	8.2	91	16	St	100	0.57	65	969.9
0700	10.8	91	2	Fog	100	0.10	Calm	970.6
0800	13.0	87	2	Fog	100	0.26	246	970.8
0900	15.2	77	16	St	50	0.98	17	971.1
1000	19.1	55	25	Clear	0	1.34	93	971.1
1100	21.3	43	25	Clear	0	1.59	67	970.6
1200	23.7	34	25	Clear	0	1.39	31	970.1
1300	25.2	21	25	Clear	0	1.95	89	969.6
1400	26.7	21	25	Clear	0	1.49	351	969.0
1500	27.6	18	25	Clear	0	1.39	59	968.5
1600	27.4	17	25	Clear	0	2.36	57	968.1
1700	26.1	20	25	Clear	0	3.03	49	968.3
1800	24.3	23	25	Clear	0	1.18	50	968.3
1900	19.6	41	25	Clear	0	0.26	220	968.5
2000	18.5	45	25	Clear	0	1.13	137	969.0
2100	16.3	54	25	Clear	0	0.72	162	969.3
2200	15.2	59	25	Clear	0	0.51	105	969.5
2300	12.7	75	25	Clear	0	0.36	36	970.0
2400	12.3	81	25	Clear	0	0.21	Calm	970.0

Table 3. Model Conditions Assumed for Leaf Temperature Calculations

PARAMETER	VALUE
Surface Albedo	0.15
Leaf Width	5 cm
Diffusion Resistance	6 cm/sec
Leaf Absorptance	
Direct Solar	0.6
Diffuse Solar	0.6
Leaf IR Absorptivity	0.97
Leaf IR Emissivity	0.97

3.2.2.1 Impact of Evapotranspiration

Figure 9 displays the leaf temperatures with and without evapotranspiration considered. The air temperature is also shown for reference. The Figure shows that, in general, leaf temperatures are lower with evapotranspiration considered than with it neglected. During the period of peak solar loading, the neglect of evapotranspiration can lead to differences in the calculated leaf temperature of as high as eight degrees.

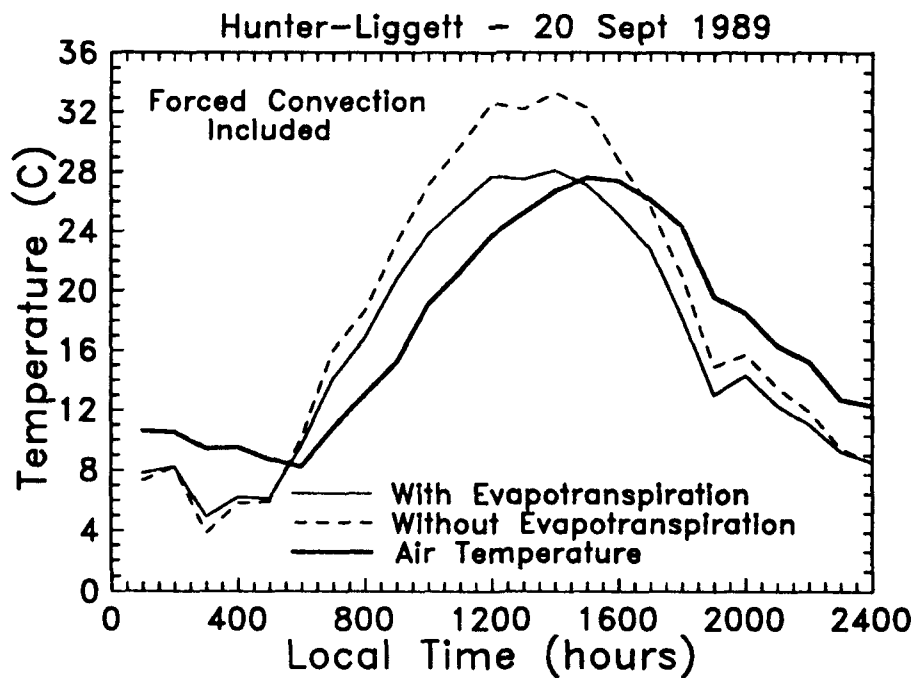


Figure 9. Leaf Temperatures Calculated With and Without Evapotranspiration for Weather Conditions Representative of the FY 90 SWOE Hunter-Liggett Demonstration

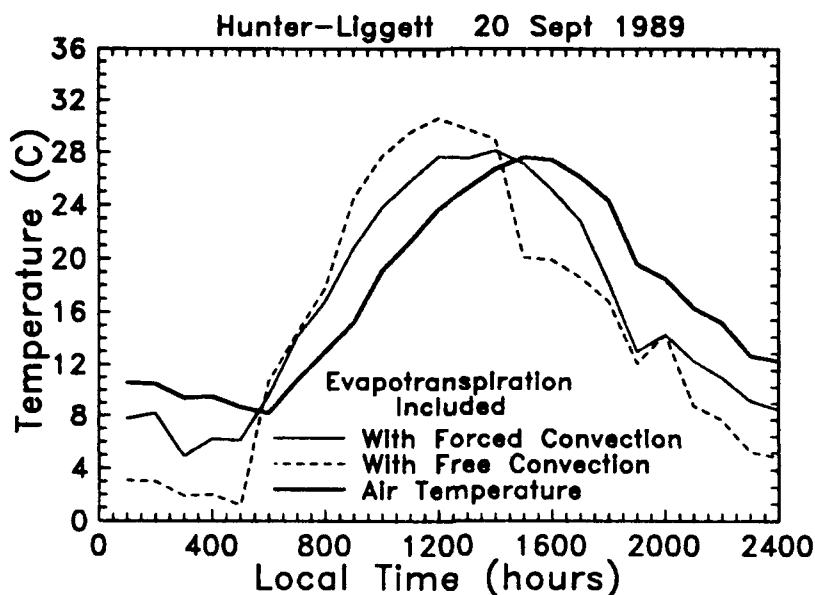


Figure 10. Leaf Temperatures Calculated With Free and Forced Convection Assumed for Weather Conditions Representative of the FY 90 SWOE Hunter-Liggett Demonstration

3.2.2.2 Impact of Convection

Figure 10 displays the leaf temperatures with free and forced convection considered. The air temperature is also shown for reference. The free convection results were obtained by setting the wind speeds to zero. With free convection assumed, the leaf temperature generally follows the variations in solar loading. With forced convection assumed, the leaf temperature also varies in response to the wind speed.

3.2.2.3 Impact of Leaf Diameter

Figure 11 displays the leaf temperatures with three different leaf diameters considered. The results show that the leaf temperature is relatively insensitive to the assumed leaf diameter.

4 VALIDATION EFFORTS

4.1 Overview of STAMP

To aid in the development of the 3-D tree model, SPARTA designed and conducted a measurement program that was held near Bangor, Maine. The purpose of this field test program was to provide a database for validation efforts and to aid in identifying important phenomenology.

A bigtooth aspen on land owned by the International Paper Company was selected for study. The measurement program was held 6 - 24 September 1990 and occurred in conjunction with a NASA program on Forest Ecosystem Dynamics.

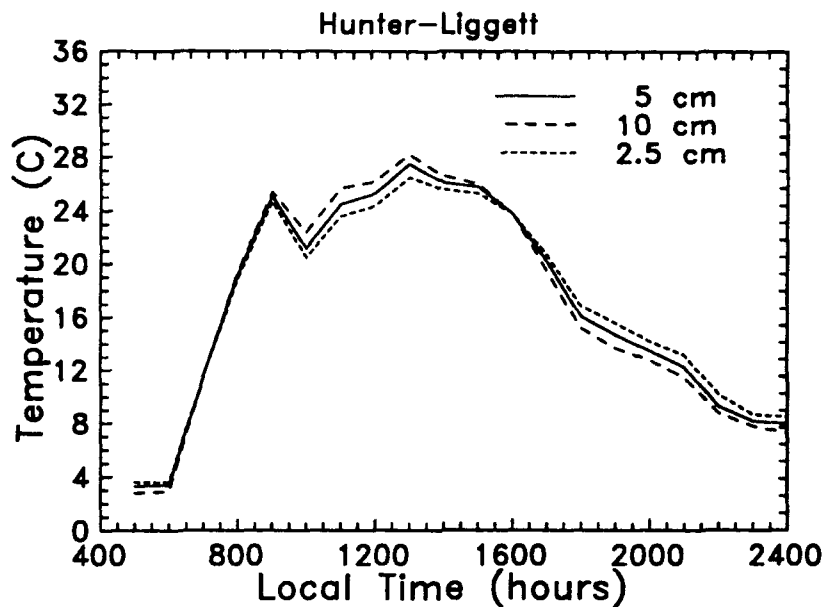


Figure 11. Leaf Temperatures Calculated With Different Leaf Diameters Assumed for Weather Conditions Representative of the FY 90 SWOE Hunter-Liggett Demonstration

The aspen tree, nicknamed Joyce Kilmer (after the poet), was instrumented with thermocouples and thermistors to measure the temperature at various locations within the tree. Leaf and bark samples were also taken and optical measurements made.¹⁷ Supporting weather data were provided by the University of Maine and imagery data were taken by personnel from the Keweenaw Research Center of the Michigan Technical University.

4.2 Discussion of Results

In this section, the TREETHERM model will be used to predict temperatures at various locations in a tree trunk. Results will be given for comparison against the Maine tree, "Joyce Kilmer", and a tree located at Hunter-Liggett, California. This was the site being modeled for the demonstration effort in the second year of SWOE.

¹⁷ Neu, J.T., Dummer, R.S., Beecroft, M., McKenna, and Robertson, D.C. (1990) "Surface Optical Property Measurements on bark and Leaf Samples," Geophysics Laboratory, Hanscom AFB, Massachusetts, PL-TR-91-2009

4.2.1 Temperature Predictions for "Joyce Kilmer"

A cross-section of the trunk ≈ 4.5 " in diameter at the one foot level was modeled. Little to no shading occurred from other branches or leaves at this location. Meteorological data from 8 and 9 September 1990 were used to calculate the solar and downward infrared boundary conditions. The meteorological data were taken at a site immediately adjacent to the tree. Weather conditions were generally clear on those days with daytime maximum temperatures near 20 C and nighttime minimum temperatures between 1 - 5 C.

Temperature predictions from TREETHERM have been compared against thermocouple data taken at locations on the north and south faces at about 1" in from the bark surface. Comparisons for two days of the model results and measured values are shown in Figures 12 and 13, respectively. Additionally, Figures 14 and 15 show the predicted temperature cross section distributions at 9 AM and 3 PM for 9 September 1990. In general, the agreement between the model and data are good but some model limitations are apparent. For example, the peak tree temperature is overpredicted by the model which then leads to a consistent overprediction during the rest of the day. This overprediction could be the result of a number of factors such as incorrect material properties, the inability to account for water vapor condensing on the bark (a process that occurred during the early morning), and uncertainties in the solar and infrared fluxes.

The average convective term implemented does not predict the temperature plateaus from the south face thermocouple data on both 8 and 9 September 1990. On 8 September 1990, the wind during the period 9 AM to 6 PM varied from easterly to southerly. For the same period on 9 September 1990, the wind was mostly southerly. The thermocouple data shows this by the leveling off of the temperatures at the south face thermocouple location. The wind effects are not as pronounced in the north face thermocouple data as that location was generally in the lee of the wind. Modeling the effect of the wind direction would improve the modeling of the forced convective term for exposed trunks and branches. Refinement of the forced convective term further than accounting for the wind direction and possibly the angle of incidence is not contemplated. Any effects due to the three dimensional disturbances in the velocity field are beyond the scope of this model.

The model also did not predict the abrupt morning temperature rise very well on 8 September 1990 but did a better job on 9 September 1990. This is most likely a consequence of the choice of material properties and the estimation of the incident energy on the model surface.

Comparison of the thermocouple data to predictions showed some of the difficulties in this type of modeling. There are uncertainties in the meteorological

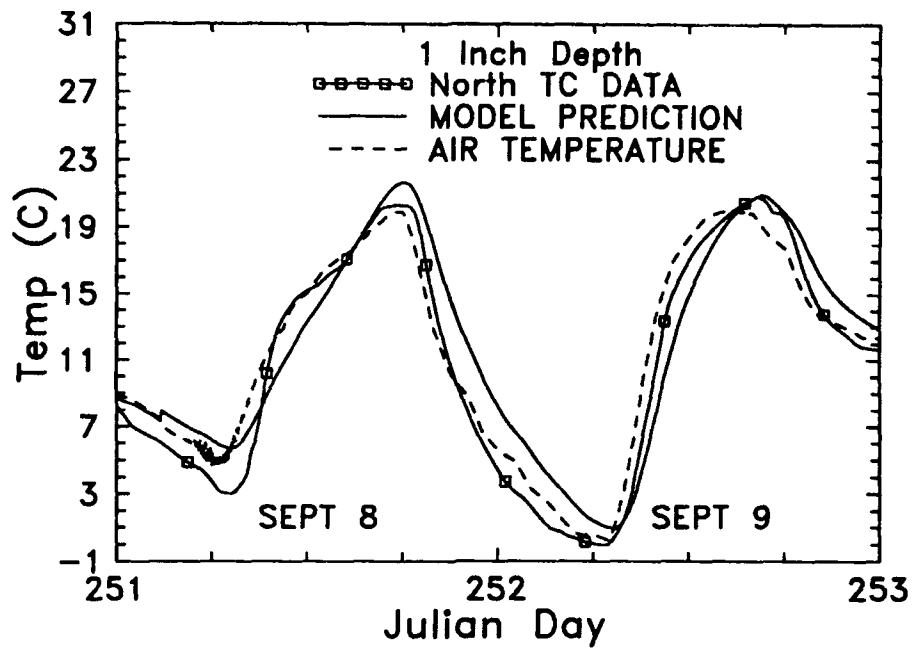


Figure 12. Tree Model Predictions for and Thermocouple Data From "Joyce Kilmer" for 8 and 9 September 1990. Data are from the northern side about 1" from the trunk surface

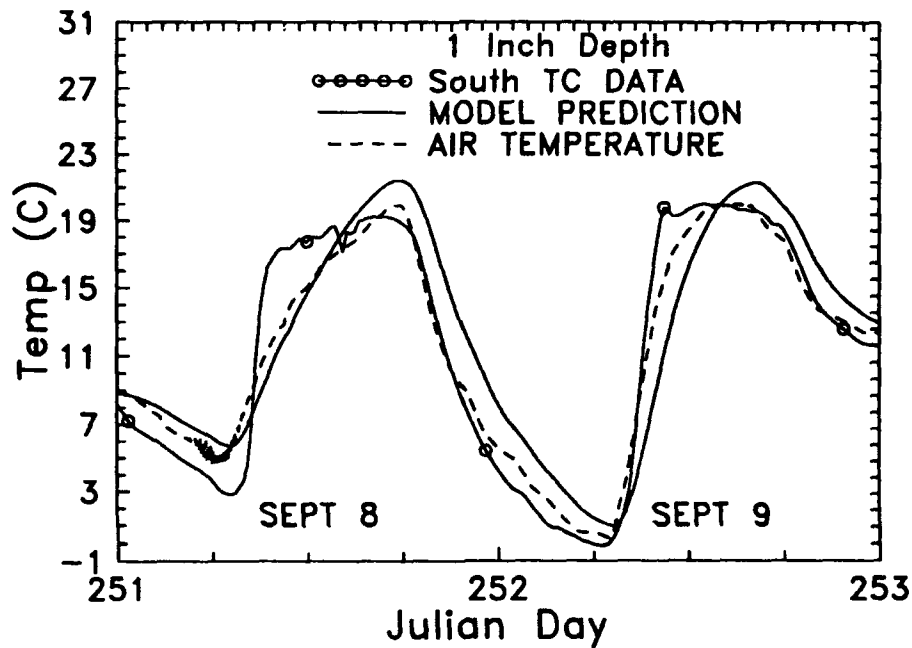


Figure 13. Tree Model Predictions for and Thermocouple Data From "Joyce Kilmer" for 8 and 9 September 1990. Data are from the southern side, about 1" from the trunk surface

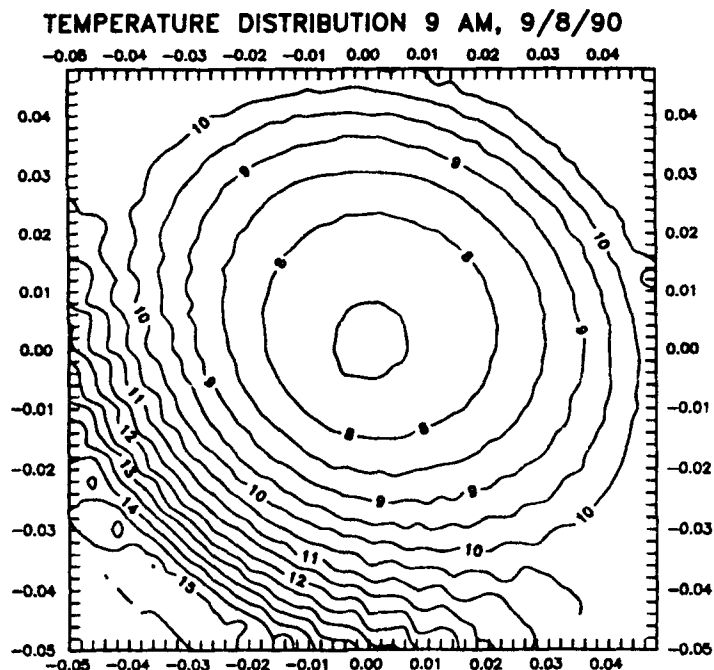


Figure 14. Model Temperature Cross Sections for "Joyce Kilmer" at 9 AM on 9 September 1990. Results are for a trunk slice at the 1 foot level. North is to the right and east is at the bottom of the figure

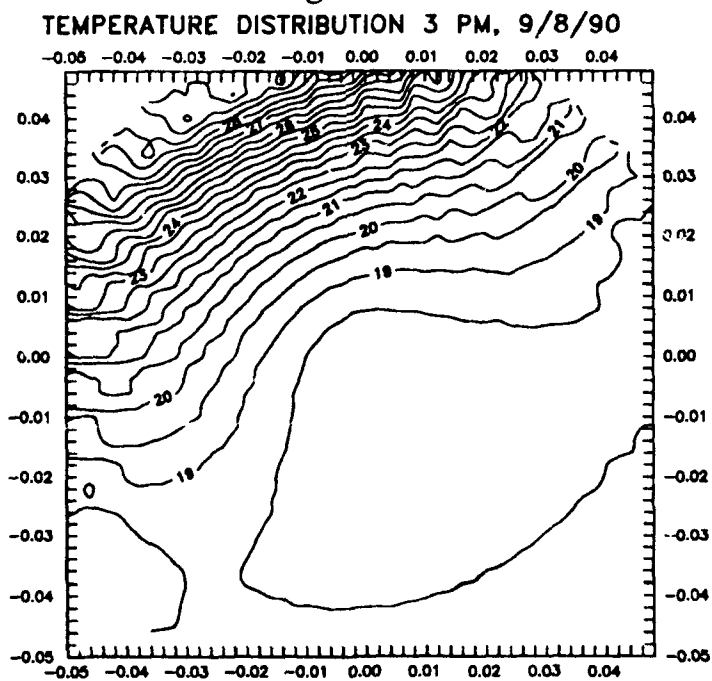


Figure 15. Model Temperature Cross Sections for "Joyce Kilmer" at 3 PM on 9 September 1990. Results are for a trunk slice at the 1 foot level. North is to the right and east is at the bottom of the figure

data, tree material properties, and internal material distribution. Moisture transport effects on the model thermal response was also not considered. Reducing the controllable uncertainties in meteorological data, refining the forced convective term, and obtaining a better representation of the material properties will overcome some of the model limitations.

4.2.2 Trunk Temperatures for Hunter-Liggett Tree

A representative cross-section of the main trunk of a mountain oak located at Hunter-Liggett, California was modeled. This tree was selected as a representative tree at the site modeled for the second year demonstration in the BTI/SWOE program. Meteorological data for 18 - 20 September 1989 from this site were used to estimate the solar and downward infrared fluxes. Figure 16 gives the temperatures as a function of time for surface elements corresponding to the cardinal compass points.

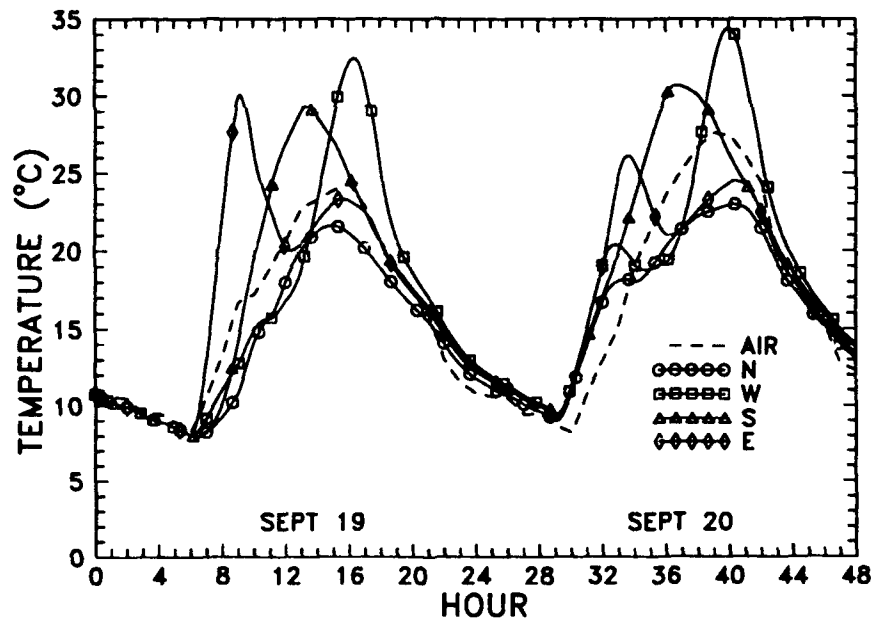


Figure 16. Predictions of the Surface Temperatures as a Function of Time for Elements Near the Cardinal Points. Calculations were made for meteorological conditions for 19 - 20 September 1989 at Hunter-Liggett, California

The impact of the fog during the morning of 20 September 1989 (see Table 3) on the model thermal response can be seen in a comparison of the temperature predictions between the mornings of 19 and 20 September 1989.

On 20 September 1989, the temperature at the cardinal points tended to rise at about the same pace until the fog burned off. This is a result of the way the

model treats infrared and diffuse solar energy. These terms are implemented as radially symmetric to the modeled cylindrical geometric shapes. In addition, the magnitude of these terms is higher for the fog conditions of 20 September 1989 than for the clear conditions of the previous morning. The dip in the north and west temperatures starting at about 8 AM is a combination of the fog cover burning off and an increase in the wind velocity.

The effects of clear conditions on 19 September 1989 and solar position on the model temperature predictions are shown at the east and west location. The calculated east temperature rises in the morning until that location becomes shaded. The west location does not receive direct solar energy until the mid-afternoon. Its temperature rise in the morning is due to diffuse solar energy, conduction, and convection due to wind.

To demonstrate the effect of solar position on the temperature distribution, contour plots of TREETHERM's temperature predictions through a cross section were made for 9 PM and 3 PM for 20 September 1989. These are shown in Figures 17 and 18. The highest thermal gradients are in the location corresponding to the solar vector. Heating (or cooling) in the shaded section is accomplished by the surface interaction with infrared radiation, wind, and the diffuse component of the solar energy.

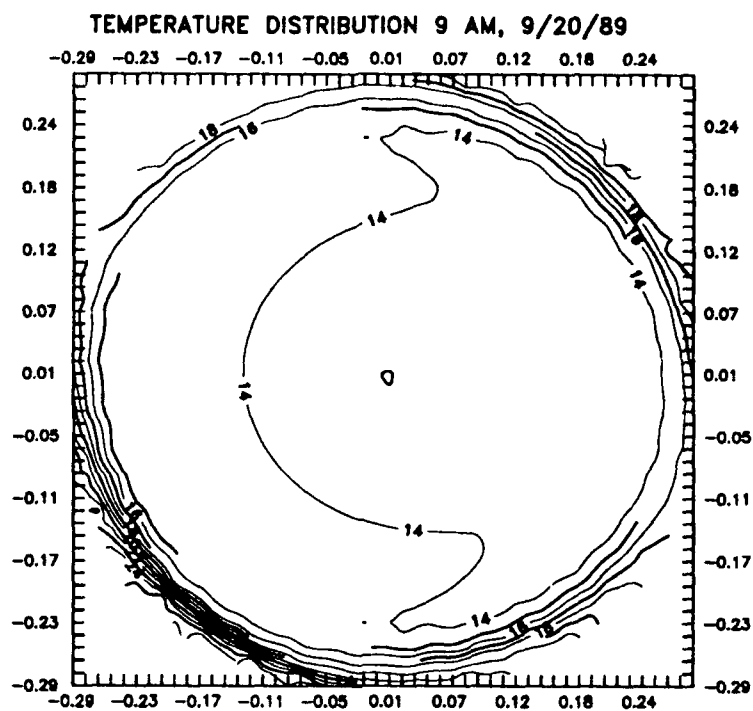


Figure 17. Model Temperature Cross Sections for 9 AM, 20 September 1989.
North is to the right and east is at the bottom of the figure

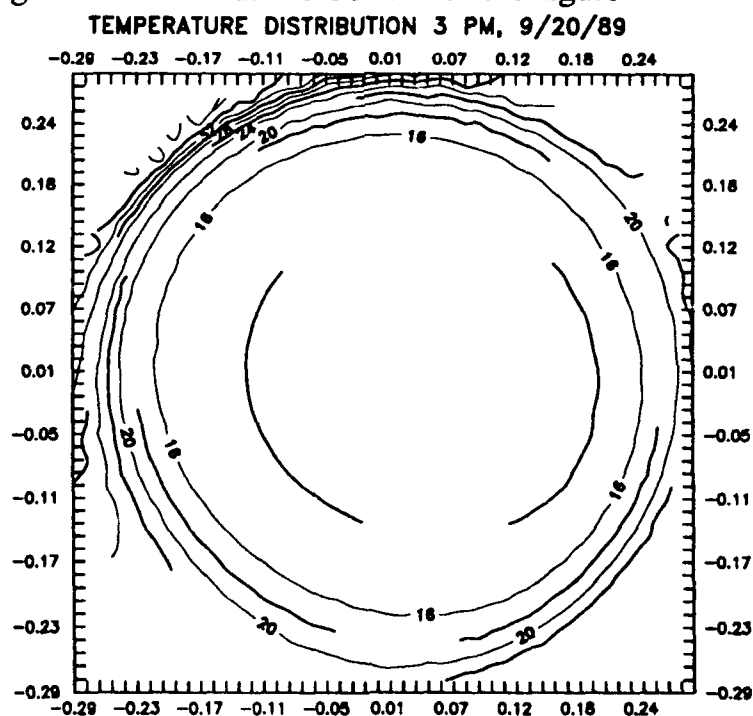


Figure 18. Model Temperature Cross Sections for 3 PM, 20 September 1989.
North is to the right and east is at the bottom of the figure

5 SUMMARY AND RECOMMENDATIONS FOR FUTURE WORK

5.1 Summary

A first generation 3-D tree thermal model, TREETHERM, has been developed for the Balanced Technology Initiative on Smart Weapons Operability Enhancement Program for use in scene simulation studies. The model can also be used in remote sensing and climate studies. TREETHERM describes a single tree in terms of primitive shapes and includes the variation in material properties. The tree reproduces the thermal response phenomenology as studied during a field test program conducted in conjunction with NASA's Forest Ecosystem Dynamics program.

TREETHERM predicts the overall thermal trends in an individual tree reasonably well. The model demonstrates the thermal response of woody materials and leaves to changes in solar loading, wind speed and direction, and evapotranspiration. However, additional development efforts are planned to refine and improve the model. Specific efforts will include the incorporation of a formulation for internal moisture flow, enhancements to the leaf energy budget model, and interactions with other objects such as adjacent trees or other objects.

5.2 Recommendations for Future Work

5.2.1 Addition of Woody Material Moisture Transport

A full moisture treatment within the tree was not included in this version of TREETHERM due to the complexity of describing the moisture content of woody material and its relationships to environmental conditions. Instead, the moisture content in the woody material was approximated and the material properties of dry wood adjusted and then kept constant during the calculations. While acceptable for a first order development effort, this is not acceptable for a model intended to fully represent a tree's response to changes in environmental conditions.

The moisture content of trees can change during the course of a day as a result of evapotranspiration processes and in result to changes in general weather conditions, such as the presence of precipitation. A first order treatment could include a temporal variation in material thermal properties. A more detailed treatment, however, would require the development of a mass balance model for the tree.

5.2.2 Enhancements to the Leaf Energy Budget Model

The leaf energy budget model utilized a number of simplifications that should be readdressed in a second generation model. First, the leaf energy budget calculations were performed for leaves assumed to be fully exposed to the sun. In an actual tree, the amount of sunlight reaching inner leaves will be attenuated by the presence of intervening leaf clusters. The full tree model has the capability to keep track of individual leaf clusters and their ability to shade other portions of the tree. This

feature should be coupled to the leaf energy budget model to correctly account for the solar loading on individual leaf clusters.

Second, the convective exchange term needs to be revised to account for different shaped leaves. The first generation model assumed circular plates for the leaves. Other shapes should be included to more accurately represent the variation in leaf morphology.

Finally, the evapotranspiration term needs to be reexamined. In particular, the temporal and environmental variability in the rate of water vapor diffusion needs to be included.

5.2.3 Tree-Environmental Interactions

This study focused on the energy budget aspects of tree-environmental interactions. There are other aspects of this interaction that deserve treatment in future versions of the model. One is the effect of the tree on wind fields near the surface. In addition to providing a source of solar shading to the ground, trees can provide a form of wind shading. That is, the presence of trees (or any 3-D object) will moderate the wind field near the surface and this modification could potentially have an impact on the convective energy exchange at and near the surface.

A second interaction deserving further study is the thermal interaction of the tree with the ground and vice versa. The upwelling ground infrared flux is a significant term in the tree and leaf energy budgets. In the present version, it was not explicitly included but, instead, the infrared sources were treated as coming from a spherically symmetric source. This was done because the inclusion of upwelling infrared sources requires that the tree be coupled to a full, three dimensional model of the surrounding environment including a treatment that accounts for shading effects from the tree and any other objects.

References

1. Hummel, J.R., Longtin, D.R., Paul, N.L., and Jones, J.R. (1991) "Development of the Smart Weapons Operability Enhancement Interim Thermal Model," Phillips Laboratory, Hanscom AFB, Lexington, Massachusetts, PL-TR-91-2073, 1991.
2. Jones, J.R. (1991) "User's Guide for TREETHERM: A 3-D Thermal Model for Single Trees," Phillips Laboratory, Hanscom AFB, Massachusetts, PL-TR-91-2109, 31 March 1991.
3. West, H.W., and Allen, H.H. (1971) "A Technique for Quantifying Forest Stands for Management Evaluations", US Army Engineer Waterways Experiment Station, Vicksburg, MS, Technical Report M-71-9, December 1971.
4. Guivens, Jr., N.R., and Henshaw, P.D. (1986) "Laser Radar Sensor Model," SPARTA, Inc., Lexington, MA, SPARTA LTR-86-08, 27 June 1986.
5. Guivens, Jr., N.R., and Henshaw, P.D. (1986) "Laser Radar Sensor Simulation," SPARTA, Inc., Lexington, MA, SPARTA LTR-87-011, 26 November 1986.
6. Henshaw, P.D., and Guivens, Jr., N.R. (1987) "Active/Passive Multiwavelength Imaging Sensor Simulation," *Laser Radar II*, R. J. Becherer and R. C. Harney, Ed., Proc. SPIE **783**:84-90.
7. Derby, R.W., and Gates, D.M., (1966) The Temperature of Tree Trunks - Calculated and Observed, *Amer. J. Bot.*, **53**:580-587.
8. Carnahan, B. Luther, H.A., and Wilkes (1969) Applied Numerical Methods, Wiley & Sons, New York, p.451.
9. Duncan, T.C., Farr, J.L., Wassel, T., and Curtis, R.J., Satellite Laser Vulnerability Model, Thermal Model User's Guide, Air Force Weapons Laboratory, (Software Documentation).
10. Churchill, S.A., and Bernstein, M. (1977), A Correlating Equation for Forced Convection from Gases and Liquid to a Circular Cylinder in Crossflow, *J. Heat Transfer*, **99**:300-306.
11. Lienhard, J. M., (1981), A Heat Transfer Textbook, Prentice-Hall, Englewood Cliffs, NJ, 1981, pp 326-337.
12. Giedt, W. H., (1949), Investigation of Variation of Point Unit Heat-Transfer Coefficient Around a Cylinder Normal to an Air Stream, *Trans. ASME*, **71**:375-381.
13. Churchill, S. W., (1977), A Comprehensive Correlating Equation for Laminar, Assisting, Forced and Free Convection, *AIChE Journal*, **23**:10-16.
14. Gates, D.M. (1964) "Characteristics of Soil and Vegetated Surfaces to Reflected and Emitted Radiation," Proceedings IGARD Symposium on Remote Sensing

of Environment, 573-600.

15. Hummel, J.R., and Reck, R.A. (1979) A Global Surface Albedo Model, *J. Appl. Meteor.*, **18**:239-253.
16. Gates, D.M., Kegan, H.J., Schleter, J.C., and Weidner, V.R. (1965) Spectral Properties of Plants, *Appl. Optics*, **4**:11-20.
17. Neu, J.T., Dummer, R.S., Beecroft, M., McKenna, and Robertson, D.C. (1990) "Surface Optical Property Measurements on bark and Leaf Samples," Geophysics Laboratory, Hanscom AFB, Massachusetts, PL-TR-91-2009

Appendix A

Tree Shading Model

The tree shading model uses ray casting technology implemented for rendering images or signatures of various objects as observed by optical sensor systems. The constructive solid geometry model in SENSORSIM has been considerably simplified for the current application, so that trees are represented by a series of coaxial pairs of cylinders, the inner cylinder of each pair representing a volume of branch (or trunk) and the outer cylinder representing a volume filled to some density with leaves. The model determines the effective illuminated area for each section of the branch attenuated for partial shading by leaves. The model adaptively determines the extent (length and width) and density of the rays according to the location and size of each branch and leaf volume. The remainder of this section describes the components of this model in greater detail.

A-1. Ray Casting Process

The ray casting process consists of generating a grid of rays corresponding to various lines of solar illumination (from the sun to the tree) and determining what part of the tree is illuminated by each ray. The tree shading model adaptively determines the extent of the ray grid and the density of rays in each region of the grid according to the location and size of the cylinders representing the tree. Since the number of rays which must be cast is roughly proportional to the number of cylinders used to model the tree and each ray must be intersected with each cylinder, the execution time for the shading model will be approximately proportional to the *square* of the number of cylinders used to model the tree.

A ray along the line of solar illumination can be represented by a point on the line (called the "ray origin") and a direction vector parallel to the line (called the "ray direction").* In vector form, any ray is given by the locus of points

* Mathematically, the terms "ray" and "line" are not synonymous; a "line" extends to infinity in both directions, while a "ray" begins at a defined point and extends to infinity in only one direction. Mathematicians additionally apply the term "half line" to a ray with the end point removed. All three of these elements can be represented by Eqn (A-1), with appropriate restrictions on the value of the ray coordinate $k \in \mathbb{R}$: $0 < k < \infty$ for a half line, $0 \leq k < \infty$ for a ray, and $-\infty < k < \infty$ for a line. In practice, rays originating at large distances from the target, and implementation considerations of processing precision dictate that the ray origin should be offset to a convenient location in the proximity of the target. As a consequence of this offset, negative values of k will ordinarily occur and do in fact correspond to valid intersection points; thus, the terms "ray" and "line" will

$$\mathbf{X}(k) = \mathbf{X}_o + k\Delta\mathbf{X} \quad (\text{A-1})$$

where $\mathbf{X}(k)$ is a point on the line, \mathbf{X}_o is the ray origin, $\Delta\mathbf{X}$ is the ray direction vector, and k is the ray coordinate of point $\mathbf{X}(k)$. The vectors in Eqn (A-1) can be separated into their respective components

$$\mathbf{X}(k) = [x(k) \quad y(k) \quad z(k)] \quad (\text{A-2a})$$

$$\mathbf{X}_o = [x_o \quad y_o \quad z_o] \quad (\text{A-2b})$$

$$\Delta\mathbf{X} = [\Delta x \quad \Delta y \quad \Delta z] \quad (\text{A-2c})$$

to obtain the equivalent scalar parametric equations for the line

$$x(k) = x_o + k\Delta x \quad (\text{A-3a})$$

$$y(k) = y_o + k\Delta y \quad (\text{A-3b})$$

$$z(k) = z_o + k\Delta z. \quad (\text{A-3c})$$

The ray coordinate (k) uniquely identifies each point along a line of illumination, and in fact is used in the simulation to sort the intersected segments into the correct sequence.

A-2. Ray Transformations

Before a ray can be intersected with a cylinder, it must be transformed from the global (scene) coordinate system into the coordinate system of the cylinder. This transformation can be represented by a square matrix, containing the magnification and rotation information, which is multiplied by the coordinate vector, and a translation vector which is added to the result of the multiplication. A point (or any other vector representing absolute coordinates) is thus transformed by*

$$\mathbf{Y} = \mathbf{XA} + \mathbf{B} \quad (\text{A-4})$$

where \mathbf{Y} is the transformed point, \mathbf{X} is the untransformed point, \mathbf{A} is the magnification and rotation matrix, and \mathbf{B} is the translation vector. \mathbf{X} and \mathbf{Y} can be used interchangeably in this discussion as convenience dictates.

* The choice of notation in Eqn (A-4), coupled with the previous use of \mathbf{X} (and the associated \mathbf{X}_o and $\Delta\mathbf{X}$) for the line of solar illumination in Eqn (A-1) assume the forward direction of all coordinate transformations to be from scene coordinates to cylinder coordinates. Since both forward and reverse transformations are available in the simulation, either this or the reverse convention could be selected arbitrarily; for consistency of notation, this convention will be retained. If the reverse convention had been chosen (that is, if the forward direction of a transformation mapped from primitive shape coordinates to scene coordinates), the effect would have been to interchange \mathbf{X} and \mathbf{Y} in Eqns (A-4), (A-5), and (A-6), and to interchange the forward transformation matrices \mathbf{A} and \mathbf{B} with the reverse transformation matrices \mathbf{A}' and \mathbf{B}' respectively in all subsequent equations.

Table A-1. Primitive Transformations

Transformation	A	B	A'	B'
Translation	$\begin{bmatrix} 1 & 0 & 0 \\ 0 & 1 & 0 \\ 0 & 0 & 1 \end{bmatrix}$	$[-t_x \quad -t_y \quad -t_z]$	$\begin{bmatrix} 1 & 0 & 0 \\ 0 & 1 & 0 \\ 0 & 0 & 1 \end{bmatrix}$	$[t_x \quad t_y \quad t_z]$
Scaling	$\begin{bmatrix} 1/s_x & 0 & 0 \\ 0 & 1/s_y & 0 \\ 0 & 0 & 1/s_z \end{bmatrix}$	$[0 \quad 0 \quad 0]$	$\begin{bmatrix} s_x & 0 & 0 \\ 0 & s_y & 0 \\ 0 & 0 & s_z \end{bmatrix}$	$[0 \quad 0 \quad 0]$
Rotation - X Axis	$\begin{bmatrix} 1 & 0 & 0 \\ 0 & \cos \psi & -\sin \psi \\ 0 & \sin \psi & \cos \psi \end{bmatrix}$	$[0 \quad 0 \quad 0]$	$\begin{bmatrix} 1 & 0 & 0 \\ 0 & \cos \psi & \sin \psi \\ 0 & -\sin \psi & \cos \psi \end{bmatrix}$	$[0 \quad 0 \quad 0]$
Rotation - Y Axis	$\begin{bmatrix} \cos \psi & 0 & \sin \psi \\ 0 & 1 & 0 \\ -\sin \psi & 0 & \cos \psi \end{bmatrix}$	$[0 \quad 0 \quad 0]$	$\begin{bmatrix} \cos \psi & 0 & -\sin \psi \\ 0 & 1 & 0 \\ \sin \psi & 0 & \cos \psi \end{bmatrix}$	$[0 \quad 0 \quad 0]$
Rotation - Z Axis	$\begin{bmatrix} \cos \psi & -\sin \psi & 0 \\ \sin \psi & \cos \psi & 0 \\ 0 & 0 & 1 \end{bmatrix}$	$[0 \quad 0 \quad 0]$	$\begin{bmatrix} \cos \psi & \sin \psi & 0 \\ \sin \psi & \cos \psi & 0 \\ 0 & 0 & 1 \end{bmatrix}$	$[0 \quad 0 \quad 0]$

fication and rotation matrix, and **B** is the translation vector. The inverse of this transformation is obtained by solving Eqn (A-4) for **X**

$$\mathbf{X} = \mathbf{Y}\mathbf{A}^{-1} - \mathbf{B}\mathbf{A}^{-1} \quad (\text{A-5})$$

The inverse transformation can thus be represented by

$$\mathbf{X} = \mathbf{Y}\mathbf{A}' + \mathbf{B}' \quad (\text{A-6})$$

where

$$\mathbf{A}' = \mathbf{A}^{-1} \quad (\text{A-7a})$$

$$\mathbf{B}' = -\mathbf{B}\mathbf{A}^{-1}. \quad (\text{A-7b})$$

The values of **A**, **A'**, **B**, and **B'** for the primitive transformations are shown in Table A-1.

A rule for combining two transformations may easily be derived by letting subscripts 1 and 2 be applied to the transformation matrices to designate the two transformations to be combined, and the unsubscripted matrices designate the combined transformation. The forward and reverse composite transformations are given by

$$\mathbf{Y} = (\mathbf{X}\mathbf{A}_1 + \mathbf{B}_1) \mathbf{A}_2 + \mathbf{B}_2 \quad (\text{A-8a})$$

$$\mathbf{X} = (\mathbf{Y}\mathbf{A}'_2 + \mathbf{B}'_2) \mathbf{A}'_1 + \mathbf{B}'_1 \quad (\text{A-8b})$$

Performing the matrix algebra necessary to obtain the form of Eqns (A-4) and (A-6),

$$\mathbf{A} = \mathbf{A}_1 \mathbf{A}_2 \quad (\text{A-9a})$$

$$\mathbf{A}' = \mathbf{A}'_2 \mathbf{A}'_1 \quad (\text{A-9b})$$

$$\mathbf{B} = \mathbf{B}_1 \mathbf{A}_2 + \mathbf{B}_2 \quad (\text{A-9c})$$

$$\mathbf{B}' = \mathbf{B}'_2 \mathbf{A}'_1 + \mathbf{B}_1' \quad (\text{A-9d})$$

This derivation makes no assumptions about the transformations being combined, so these rules may be used recursively to compute arbitrary combinations of transformations.* In the tree shading model, three transformations are applied for each cylinder, consisting of (1) translating the coordinate origin to the center of the cylinder, (2) rotating the coordinate system to coincide with the axes of the cylinder (using a precomputed rotation matrix composed of several primitive rotations), and (3) scaling to the cylinder to the proper dimensions (the horizontal (x and y) components are scaled by half the radius of the cylinder, and the vertical (z) component is scaled by half of the height).

A-3. Ray-Cylinder Intersections

The untransformed cylinder has a radius of one unit and a height of two units, and is centered at the origin of its local coordinate system. The axis of the cylinder is the vertical (z) axis. This cylinder has a volume of 3π cubic meters, and is characterized by the inside-outside function

$$f(x, y, z) = \max\left(\frac{1}{2}(x^2 + y^2 - 1), z - 1, -1 - z\right). \quad (\text{A-10})$$

The boundary of the cylinder is the locus of points where the inside-outside function evaluates to zero.

The incident ray can be expressed by separating Eqn (14) into its respective components

$$x(k) = x_o + k\Delta x \quad (\text{A-11a})$$

$$y(k) = y_o + k\Delta y \quad (\text{A-11b})$$

* The ability to arbitrarily combine transformations by this rule is actually dependent on the associative property of the operation of combining transformations defined by Eqns (A-9a) through (A-9d). This property can be proven by using the associative and distributive laws of matrix multiplication and addition to show that $\mathbf{A} = (\mathbf{A}_1 \mathbf{A}_2) \mathbf{A}_3 = \mathbf{A}_1 (\mathbf{A}_2 \mathbf{A}_3)$ and $\mathbf{B} = (\mathbf{B}_1 \mathbf{A}_2 + \mathbf{B}_2) \mathbf{A}_3 + \mathbf{B}_3 = \mathbf{B}_1 (\mathbf{A}_2 \mathbf{A}_3) + (\mathbf{B}_2 \mathbf{A}_3 + \mathbf{B}_3)$. It is not necessary to prove the corresponding relationships for the inverse transformations because the inverse transformations are themselves valid transformations and thus governed by the same theorem.

$$z(k) = z_o + k\Delta z \quad (\text{A-11c})$$

where

$$\mathbf{Y}_o = [x_o \quad y_o \quad z_o] \quad (\text{A-12a})$$

$$\Delta \mathbf{Y} = [\Delta x \quad \Delta y \quad \Delta z]. \quad (\text{A-12b})$$

The points where the ray intersects the surface of the cylinder may be obtained by first considering the infinite cylinder represented by the first argument to the maximum function in Eqn (A-10). Setting this expression to be zero and substituting Eqns (A-11a) and (A-11b) yields an equation for the intersection of the ray with the infinite cylindrical surface of the form

$$ak^2 + bk + c = 0 \quad (\text{A-13})$$

where

$$a = \Delta x^2 + \Delta y^2 \quad (\text{A-14a})$$

$$b = 2(x_o\Delta x + y_o\Delta y) \quad (\text{A-14b})$$

$$c = x_o^2 + y_o^2 - 1. \quad (\text{A-14c})$$

If a is not zero, the roots of Eqn (13) are given by the quadratic formula

$$k = \frac{-(b/2) \pm \sqrt{(b/2)^2 - ac}}{a} \quad (\text{A-15})$$

The intersection points given by Eqn (A-15) are complex or the same whenever the ray misses (that is, does not intersect) the infinite cylinder. This condition is identified by the discriminant of the quadratic (the quantity under the square root in Eqn (A-15)). If the discriminant is negative or zero, the ray misses the cylinder and no further computation is performed; otherwise, the ray intersects the infinite cylinder in exactly one segment. Since a cannot be negative (it is the sum of the squares of two real values) and the special case where a is zero requires separate treatment, the ray coordinate corresponding to the smaller range (the point where the ray enters the infinite cylinder) is obtained by choosing the negative sign for the square root, and the ray coordinate corresponding to the greater range (where the ray exits the infinite cylinder) is obtained by choosing the positive square root.

If the ray is found to intersect the infinite cylinder, it is a simple matter to verify whether it also intersects the finite cylinder. To perform this verification, the vertical (z) component of the infinite cylinder entrance and exit points are computed by substituting the respective roots obtained from Eqn (A-15) into Eqn (A-11c). If both points are at or above the top of the finite cylinder (that is, $z \geq 1$ for both roots), the ray misses (that is, does not intersect) the finite cylinder.

The ray likewise misses the finite cylinder if both points are at or below the bottom of the finite cylinder (that is, $z \leq -1$ for both roots). In either of these cases, no further computation is necessary. In all other case, the ray intersects the finite cylinder in some subset of its intersection with the infinite cylinder.

It exactly one endpoint of the segment where the ray intersects the infinite cylinder is above the top of the finite cylinder, the corresponding endpoint of the intersection segment for the finite cylinder must be on the top of the finite cylinder. The vertical (z) coordinate of this intersection point is that of the top of the cylinder ($z = 1$, obtained by setting the second argument of the maximum function in Eqn (A-10) to zero); combining this result with Eqn (A-11c) and solving for the ray coordinate

$$k = \frac{1-z_0}{\Delta z} \quad (\text{A-16})$$

Likewise, if exactly one endpoint of the segment where the ray intersects the infinite cylinder at a point which is below the bottom of the finite cylinder, the corresponding endpoint of the segment where the ray intersects the finite cylinder is given by

$$k = \frac{-1-z_0}{\Delta z}. \quad (\text{A-17})$$

It is not necessary to consider the special case of zero values of Δz in Eqns (A-16) and (A-17), since this condition would correspond precisely to a horizontal ray which could neither enter nor exit through the top or bottom of the cylinder.

The case of a vertical ray ($a = 0$) requires special treatment, as Eqn (A-13) becomes irrelevant. (By Eqn (A-14a), a is zero if and only if both Δx and Δy are zero, in which case b is also zero by Eqn (A-14b).) In this case, the ray intersects the infinite cylinder if and only if c is negative; thus, if c is not negative, no further computation is necessary. If c is negative, the intersection points must be the top and bottom of the cylinder, and the ray coordinates can be computed directly from Eqns (A-16) and (A-17). A check of the sign of Δz is sufficient to tell whether the ray enters the cylinder at the top and exits at the bottom (Δz negative) or vica versa (Δz positive); Δz cannot be zero since the ray direction vector cannot be a zero vector.

The surface orientation vector (normal to the cylinder) in primitive shape coordinates is obtained by combining Eqn (A-10) with the relationship

$$\mathbf{N}_Y = \nabla f \quad (\text{A-18})$$

For a ray intersecting the cylindrical part of the surface, the first argument to the maximum function in Eqn (A-10) prevails and the normal vector is given by

$$\mathbf{N}_Y = [x \quad y \quad 0] \quad (\text{A-19})$$

where x and y are computed, respectively, from Eqns (A-11a) and (A-11b). For segment endpoints on the top of the cylinder, the second argument to the maximum function prevails and the normal vector is

$$\mathbf{N}_Y = \begin{bmatrix} 0 & 0 & 1 \end{bmatrix} \quad (\text{A-20})$$

Likewise, on the bottom of the cylinder, the third argument to the maximum function prevails and the normal vector is

$$\mathbf{N}_Y = \begin{bmatrix} 0 & 0 & -1 \end{bmatrix} \quad (\text{A-21})$$

Since the cylinder is defined to be a mathematical open set, the vertical coordinate of the intersection point can be used to select the correct equation for the normal vector. The normal vector is used to determine the sector of the branch which is intersected by the ray.

A-4. Effective Illuminated Area

The effective illuminated area is defined to be the area of a planar patch oriented normal to the direction of solar radiation that would receive the same incident solar radiation as a sector of a branch (or trunk). To compute the effective illuminated area for each sector of each branch, an effective area for each ray is computed by multiplying the area corresponding to each ray (the square of the ray separation in the applicable region of the ray grid) by any attenuation due to partial shadowing by leaf volumes intersected before the first intersected branch cylinder, which is assigned to the appropriate sector of the first branch cylinder intersected by the ray. The effective area for rays incident upon the ends of cylinders are neglected. For rays intersecting the cylindrical surface, the intersected sector is determined from the orientation of the surface normal vector in the local coordinate system.